# Developments in X-Ray Tomography Characterisation for Electrochemical Devices

T. M. M. Heenan[1,2], C. Tan[1,2], J. Hack[1], D. J. L. Brett[1,2] and P. R. Shearing[1,2]*

1 Electrochemical Innovation Lab, Department of Chemical Engineering, UCL, London, WC1E 7JE, UK
2 The Faraday Institution, Quad One, Harwell Science and Innovation Campus, Didcot, OX11 0RA, UK
* Paul R. Shearing, The Electrochemical Innovation Lab, Department of Chemical Engineering, University College London, WC1E 7JE, UK. Tel.: +44(0)20 7679 3783; Fax: +44 (0)20 7679 7092; E-mail: p.shearing@ucl.ac.uk

## Abstract

Over the last century, X-ray imaging instruments and their accompanying tomographic reconstruction algorithms have developed considerably. With improved tomogram quality and resolution, voxel sizes down to tens of nanometres can now be achieved. Moreover, recent advancements in readily accessible lab-based X-ray computed tomography (X-ray CT) instruments have produced spatial resolutions comparable to specialist synchrotron facilities. Electrochemical energy conversion devices, such as fuel cells and batteries, have inherently complex electrode microstructures to achieve competitive power delivery for consideration as replacements for conventional sources. With resolution capabilities spanning tens of microns to tens of nanometres, X-ray CT has become widely employed in the three-dimensional (3D) characterisation of electrochemical materials. The ability to perform multiscale imaging has enabled characterisation from system- down to particle-level, with the ability to resolve critical features within device microstructures. X-ray characterisation presents a favourable alternative to other 3D methods such as focused ion beam scanning electron microscopy, due to its non-destructive nature, which allows four-dimensional (4D) studies, three spatial dimensions plus time, linking structural dynamics to device performance and lifetime. X-ray CT has accelerated research from fundamental understanding of the links between cell structure and performance, to the improvement in manufacturing and scale-up of full electrochemical cells. Furthermore, this has aided in the mitigation of degradation and cell-level failures such as thermal runaway. This review presents recent developments in the use of X-ray CT as a characterisation method and its role in the advancement of electrochemical materials engineering.

## Key words

Lithium-Ion Battery; Polymer Electrolyte Fuel Cell; Solid Oxide Fuel Cell; X-ray Computed Tomography

# Contents

# Introduction

The depletion of carbon-intensive fuels has been accompanied by increasing pollution levels and reduced energy security. Consequently, global efforts have been made to explore alternative energy strategies. As a result, electrochemical devices will likely comprise a significant portion of the future energy market. Fuel cell and battery technologies can be developed to meet the needs of a diverse range of applications, from grid-scale electricity distribution to portable consumer electronics, as electrochemical cells are vastly scalable.

Three of the most promising devices are the lithium-ion battery (LIB), the polymer electrolyte fuel cell (PEFC) and the solid oxide fuel cell (SOFC), each device possessing unique benefits such as energy density, start-up time and capital installation costs [1-3]. LIBs offer high energy densities and immediate power without the need for a fuel tank, although the operation of LIBs through charge and discharge cycling interrupts power delivery. Since fuel cells, including PEFCs and SOFCs, employ a fuel tank, they can operate continuously provided the fuel supply is uninterrupted. PEFCs typically cannot supply immediate power like LIBs without degradation of the cell but can offer very competitive start-up times on the order of seconds to minutes. However, these cells employ expensive metal catalysts contributing considerably to the overall price of the unit. SOFCs operate at elevated temperatures permitting the use of lower cost catalysts, but high temperatures can also be accompanied by slow start-up times for planar geometries, which are often on the order of hours. This portfolio of devices, which tension performance, cost and durability benefits have the collective potential to revolutionise energy systems.

These electrochemical energy storage devices experience performance loss over their lifetimes and there has been a significant focus in both academia and industry on achieving acceptable degradation rates. One significant source of degradation and performance loss arises from changes in the device microstructure; three-dimensional (3D) characterisation can be a powerful tool in correlating microstructure and performance. Furthermore, four-dimensional (4D) characterisation, the study of 3D structures with time, allows the direct comparison between data sets. This permits individual features to be tracked during degradation, exposing the intricate developments of such mechanisms [4].

There are three main probes which are employed for 3D characterisation of electrochemical devices: focused-ion beam scanning electron microscopy (FIB-SEM), neutron computed tomography and X-ray computed tomography (X-ray CT) [5-7]. When carrying out 4D characterisation, non-destructive techniques must be employed; when collecting FIB-SEM data, the ion-beam destroys the sample, preventing 4D studies. Additionally, the restricted availability, as well as limitations in spatial and temporal resolutions, has resulted in significantly fewer studies from neutron techniques. Therefore, X-ray CT is commonly employed for non-destructive 4D studies.

X-ray CT can operate in multiple modes: absorption (absorption), phase-contrast (phase), diffraction (XRD) or fluorescence (XRF), with each technique offering unique information and bringing individual merit. This review will discuss the developments of X-ray CT techniques for the characterisation of electrochemical devices with a particular focus on LIBs, PEFCs and SOFCs.

# The Production and Use of X-rays for Materials Characterisation

X-rays are electromagnetic waves with wavelengths in the region of angstroms to nanometres and were discovered by Wilhelm Conrad Röntgen in 1895. It was later found that an anode target bombarded with electrons would emit primary X-rays characteristic of the anode material. This knowledge formed the basis of lab-based X-ray production. However, accompanying these highly defined, primary X-rays, is the production of Bremsstrahlung radiation which is generated from the deflection of an electron by the electric field of an atomic nucleus. The distance of the electron from the nucleus determines the degree of deflection,

hence the energy of the radiation emitted, therefore producing a spectrum of energies. Synchrotron radiation is produced using the principles of Bremsstrahlung radiation. However the trajectories of the electrons are extremely well-defined, allowing the production of highly monochromatic, 'tuneable' beams. Regardless of the source, X-rays are typically refined into well-defined beams depending on the spatial and/or temporal coherence requirements of a particular characterization technique. Spatial and temporal coherence of a beam are associated with the degree of collimation and monochromaticity, respectively, and beam-refinement is common in both lab and synchrotron sources.

X-ray characterisation comes predominantly in three forms: X-ray diffraction (XRD) as described by the Bragg equation, X-ray absorption as described by the attenuation coefficient, and X-ray fluorescence (XRF) as described by Moseley's law. XRD and XRF data is collected in the form of patterns with discrete intensity peaks corresponding to the crystallographic and elemental properties, respectively. On the other hand, absorption data is collected in the form of the attenuation of the X-ray intensity integrated for the entire beam-path, from source to detector. Point XRD, XRF and absorption characterisation can come in the form of single-point probing or raster-collection, or in the case of absorption, the entire region of interest (ROI) can sometimes be characterised through full field illumination via the collection of a radiograph.

In order to obtain three-dimensional (3D) data, tomographic techniques can be employed, whereby many data points are collected at multiple angles which can be later combined using reconstruction algorithms to resolve the crystal, elemental or absorption information for a single point in space. Filtered back-projection [8] reconstruction algorithms are most commonly employed to produce the reconstructed 3D datasets, which are called tomograms, and are comprised of many voxels (3D pixels), which are each assigned a number correlating to the particular characteristic metric of interest.

When choosing an instrument for X-ray characterisation two main questions should be asked: is the resolution sufficient and is the beam suitable for the materials of interest? The spatial resolution of an instrument has to be compatible with the feature size of interest, and temporal resolution can be of particular importance when performing 4D characterization of dynamic processes. Although the spatial and temporal resolutions are important, a sufficient volume of material must also be examined in order to ensure satisfactory materials statistics, i.e. the characterisation must involve a volume that is large enough to be representative of the material bulk.

The current state-of-the-art zone-plate imaging available to both lab and synchrotron facilities can achieve spatial resolutions on the order of tens of nanometres, which is the highest spatial resolution in full-field imaging [9, 10]. Moreover, the use of phase-retrieval methods [11] can significantly enhance edge features, particularly when combined with their counterpart X-ray absorption data [12]. However, ptychography techniques are principally wave-length limited and are therefore capable of resolving far smaller spatial features [13].

The suitability of an X-ray beam to study a material of interest is determined by the energy and brilliance of the incident beam. The transmission in absorption imaging, Q range in XRD and spectral range in XRF are a function of incident energy, whereas the source brilliance determines the exposure time required to achieve an acceptable signal-to-noise ratio and resulting acquisition time. Brilliance is defined as the number of photons per second, within a bandwidth of 0.1% of the central wavelength, accounting for angular divergence and the cross-sectional area of the beam, and is a common metric for comparing X-ray beam quality for tomographic imaging.

Although it is often more convenient, and practical, to conduct an internal tomography i.e. image an ROI that lies within the sample, the image quality can also be improved substantially by the use of precise sample preparation techniques. For example, FIB milling has been used substantially in the preparation of small samples [14], but the recent development of laser machining tools has seen an increase in their use [15]. The optimal sample geometry for tomographic characterisation is a cylinder, with diameter and height equal to (or marginally larger than) the field of view (FOV) for optimal statistics, although samples of a smaller diameter may be employed in order to optimise transmission to improve signal-to-noise. This geometry minimises the amount of material external to the FOV that is

not characterised, but which the X-rays must still pass through i.e. attenuation of the beam. It also maximises the volume of sample that can be analysed, thus improving the statistical representation.

Imaging artefacts may also influence image quality; for instance, absorption imaging can suffer from streaking artefacts, particularly when imaging metals; fluorescence imaging can lead to self-absorption artefacts due to the low energy ranges that photons due to XRF are produced; and peak broadening effects in larger sample when employing XRD.

A brief introduction to the properties of X-rays has been discussed here, but thorough discussions can be found by Van Grieken et al. and Assmus et al. for information beyond the scope of this review [16, 17]. Furthermore, numerous sources for information on the X-ray properties of materials exist on the National Chemical Database Service (NCDS), the National Institute of Standards and Technology (NIST) and the Centre for X-ray Optics (CXRO), which often include data libraries [18, 19].

## Electrochemical Devices

Although distinct in their qualities the PEFC, SOFC and LIB also share several similarities. Each device is comprised of the same principal components of an electrochemical cell: two electrodes electrically isolated from one another, but ionically connected via an electrolyte [20]. Despite obvious differences in the materials between each device, which will be discussed further in the subsequent sections, the transport mechanisms are analogous; ions are transported through the electrolyte from reaction sites at one electrode to reaction sites at the other electrode, while the electrons pass around an external circuit. The current from a fuel cell is provided by gases from a fuel tank, forming ions at the electrode reaction sites; whereas LIBs store the ions within the electrodes through intercalation processes [3]. All of the devices use complex porous electrodes to support the underpinning reactions; the percolation and degree of tortuosity within the transport networks is important for all three devices. The field of materials characterisation of electrochemical devices is vast due to the variety of chemistries, structures (crystal, nano, micro and macro), and feature sizes employed. Significant research has focused on optimising these materials from the particle- to cell-level in order to make improvements in fabrication and operation, to minimise degradation and ultimately to delay cell failure [21-23]. The specific materials of interest will now be discussed for each device.

### The Lithium-Ion Battery

Within the LIB, $Li^+$ is stored within the electrodes ready to be transferred from one electrode to the other during cell operation. LIBs typically operate at room temperature and employ electrolytes that are usually composed of a lithium salt such as lithium hexafluorophosphate ($LiPF_6$) in an organic aprotic solvent. Mixtures of alkyl carbonates in the form of ethylene carbonate (EC), dimethyl carbonate (DMC), diethyl carbonate (DEC) or ethyl methyl carbonate (EMC) are most commonly used as solvent [24]. A wide range of transition metal oxides have been proposed for the positive electrode, and Li-M-$O_2$ materials have been extensively researched, where M is either nickel (Ni), manganese (Mn), cobalt (Co) or a combination of the three (Eqn. 1). Considerable work has been applied to the development of new positive electrode materials as discussed by Mohanty et al. [25]. The negative electrode is typically formed of carbonaceous materials such as graphite, whereby intercalation compounds can be formed, $LiC_x$ (Eqn. 2). In efforts to increase cell capacities, the addition of alloying materials, such as silicon (Si), to graphite has been proposed, although volume expansion issues remain problematic. Many other alloying compounds can be formed and are explored by Obrovac and Chevrier [26], and pure metal electrodes have been reviewed by Larcher et al. [27].

Positive and negative electrode materials are intimately mixed with conductive carbon and binder and coated onto aluminium and copper current collectors, respectively. Finally, the electrodes are electronically isolated from each other using a non-woven or polymeric

separator to prevent internal short circuits; short circuiting can trigger thermal runaway and catastrophic failure, which is accompanied by significant safety risks. Research into separators has been reviewed by Arora and Zhang [28, 29].

Battery electrodes are an ideal candidate for 3D characterization due to their heterogeneous nature and features that span multiple length-scales; state-of-the-art active cathode materials typically consist of secondary particle agglomerates with micrometre-sized features made up of primary particles with nano-sized features, held in a porous carbon and binder matrix [30]. Electrons are conducted between active material particles and the current collectors via the porous carbon and binder matrix (carbon-binder domain or CBD), which also allows the simultaneous flow of $Li^+$ ions through the electrolyte percolated within its pores. Conductivity within LIBs has been reviewed by Park et al. [31]. For commercial applications, LIBs are fabricated in pouch, prismatic or cylindrical geometries, with double-sided electrode coatings to maximize energy density.

Equation 1 $$\mathrm{LiMO_2} \rightleftharpoons \mathrm{Li_{1-X}MO_2} + \mathrm{XLi^+} + \mathrm{Xe^-}$$

Equation 2 $$\mathrm{C} + \mathrm{XLi^+} + \mathrm{Xe^-} \rightleftharpoons \mathrm{Li_XC}$$

Irrespective of geometry, LIBs can experience a host of degradation mechanisms during operation, which can be observed in the form of subtle microstructural changes during operation or even by catastrophic failure during thermal runaway. Thermal runaway is a significant safety concern for LIB use, and it can be described as a cascade of reactions triggered after a critical temperature is reached via either the supply of heat from an external source, mechanical damage or abnormal electrical conditions (or any combination of these) [32]. The voltage range and C-rate are two key operating parameters for LIBs, and along with storage and operating temperature ranges, can determine the mechanisms of degradation. For instance, overcharging a LIB, i.e. removing too much lithium from the structure of some transition metal oxide compounds, can trigger irreversible changes in their crystallography due to oxygen loss [33, 34]. Similarly, operating at C-rates above the capabilities of the materials employed can result in lithium plating, dendrite formation and overheating of the cell. If dendrites grow large enough they can perforate the separator triggering an internal short circuit and thermal runaway. During failure, many nano-, micro- and macrostructural changes can be expected to occur: from particle cracking to side-wall rupture, the length-scale of degradation features of LIBs can vary [35].

## The Polymer Electrolyte Fuel Cell

PEFCs operate at temperatures below 100 °C and yield a current through the oxidation of hydrogen at the anode (Eqn. 3) producing protons, which travel through the electrolyte to be reduced with oxygen yielding water at the cathode (Eqn. 4) while electrons are forced to travel around an external circuit [1]. The main function of the PEFC membrane is to transport protons from the anode to the cathode, so membranes are fabricated as thin as possible (< 50 µm) to minimise the resistance to proton conduction [36]. PEFC membranes are polymers that typically contain sulfonic groups. One of the most commonly used membranes is Nafion: a polymer with a polytetrafluoroethylene acid (PTFE) backbone and fluorodiether side-chains with sulfonic acid end-groups. The sulfonic acid end groups facilitate proton transport, as well as ensuring the membrane can stay hydrated [37, 38]. The presence of water in the membrane allows the formation of hydronium ions ($H_3O^+$), and this mechanism in combination with the hopping of protons along the sulfonic groups facilitates the transport of protons through the membrane.

Equation 3 $$\mathrm{2H_2} \rightleftharpoons \mathrm{4H^+} + \mathrm{4e^-}$$

Equation 4 $$\mathrm{O_2} + \mathrm{4H^+} + \mathrm{4e^-} \rightleftharpoons \mathrm{2H_2O}$$

The PEFC membrane electrode assembly (MEA) is usually symmetrical in structure, consisting of the polymeric membrane surrounded by two gas diffusion electrodes (GDEs). Each GDE comprises a catalyst layer (CL) in direct contact with the membrane, a microporous layer (MPL) and supported by a gas diffusion layer (GDL). Finally, a gasket frames the active area of the GDE on each side and the cell is assembled under compression with bipolar plates [39]. The CL is the location where the electrochemical reactions occur [40] and typically consists of platinum-on-carbon nanoparticles, although, non-precious metal catalysts are also being developed [41]. CLs are typically thin (tens of microns), with low catalyst loadings, to reduce the amount of precious catalyst and improve mass transport. However, reducing the CL thickness and loading also reduces the number of electrochemical reaction sites. Catalyst nanoparticles are small (ca. 3 – 8 nm) and highly dispersed, which maximises the number of catalytically active sites available for reactions. The MPL and GDL permit electrical conduction to and from the reaction sites, as well as allowing multiphase reactants and products to permeate through the microstructural network. The MPL aids particularly in liquid transport and is often formed of carbon black powder with a fine nanoporous structure. The GDLs are relatively thick (100 – 300 μm) and are typically composed of carbon fibres either woven into a cloth or bonded using resins to form carbon paper [37]. Bipolar plates are generally graphitic or metallic to provide good conductivity for current collection. They are also etched with often complex gas flow channels, which facilitates mass transport of the reactants and products into and out of the fuel cell [42]. Pore sizes in the MPL and GDL are tuned to enable efficient transport of water away from the cathode into the channels of the bipolar plates and out through the exhaust stream, thus avoiding flooding. The locations where the reactions occur are named the triple-phase boundaries (TPB) and require the presence of the catalyst to promote the reaction, conductive carbon to transport the electrons and a percolated pore to provide/remove the reactants/products. The site must also be able to facilitate proton transport via one of the aforementioned mechanisms. The electrochemical surface area (ECSA) correlates strongly with the electrochemical power density and is often used as a comparison for cell performance. PEFCs can suffer performance losses due to several structural issues: perforation of the membrane during fabrication or operation can cause gas cross-over reducing the cell potential [43], moreover, membrane drying, contamination or mechanical stress while under non-uniaxial compression [29] can all contribute to undesirable overpotential. The CL can experience a loss of catalytic activity due to degraded catalyst particles via sintering, agglomeration, corrosion, Pt-dissolution and mechanical stress. Other loss mechanisms in the CL include corrosion of the carbon support through undesired carbon oxidation. Morphological changes in the CL arising as a result of this degradation, such as collapse of the pore structure or loss of the carbon support entirely, result in a reduction of electrochemical performance [44]. The affinity of platinum to carbon monoxide (CO) is particularly problematic for the activity of the CL; CO is often found in trace amounts in hydrogen produced by steam methane reforming and adsorbs readily onto the CL Pt surface, which blocks reactant sites [37]. Losses in mass transport and conductivity can occur within the MPL and GDL due to degradation of the backing materials, mechanical stress (often induced through thermal cycling), and hydrophobicity changes triggered by corrosion [45]. Therefore like the LIB, the PEFC can experience many complex degradation mechanisms across multiple time and length scales.

## The Solid Oxide Fuel Cell

The SOFC operates via the transport of $O^{2-}$ ions from the reduction of oxygen at the cathode (Eqn. 5), through the electrolyte to the oxidation of hydrogen at the anode producing water (Eqn. 6) [2]. SOFCs operate at temperatures in the range of 600 – 1000 ºC, significantly higher than both LIBs and PEFCs.

Equation 5 $$O_2 + 4e^- \rightleftharpoons 2O^{2-}$$

Equation 6 $$2H_2 + 2O^{2-} \rightleftharpoons 2H_2O + 4e^-$$

Materials with fluorite structures, such as zirconia ($ZrO_2$) or ceria ($CeO_2$) based ceramics, are typically employed as the electrolyte. These ceramics are doped to increase the concentration of oxygen vacancies: zirconia is typically stabilised with 8 mol% yttria forming $(Y_2O_3)_{0.08}(ZrO_2)_{0.92}$ (YSZ), whereas, ceria is commonly doped with 10 mol% gadolinium to give $Ce_{0.9}Gd_{0.1}O_{1.95}$ (CGO or GDC) [46]. The oxide conduction within the electrolyte is facilitated by the oxide ion vacancies and interstitial oxide ions. The electrolytes must be dense with very low porosities to prevent crossover of either of the reactant gases, as this would reduce the open circuit potential because of undesirable stoichiometry.

Anodes are generally formed from metal-ceramic (cermet) composite materials such as nickel (Ni) and YSZ, forming Ni-YSZ. The metal acts as the catalyst and a transport network for the electrons, whereas, the ceramic provides the pathways for ionic transport. The location where the metal, ceramic and pore meet are thought to be the location of the reaction sites namely the triple-phase boundary (TPB) [2], analogous to the PEFC. The volumetric density ($\rho_{TPB}$) of these sites is used as a benchmark for performance, as it correlates strongly with the electrochemical power density.

Cathodes are typically ceramic oxides with perovskite structures such as strontium-doped lanthanum manganite, $La_{0.7}Sr_{0.3}MnO_3$ (LSM), or strontium-doped lanthanum cobalt ferrite, $La_{0.6}Sr_{0.4}Co_{0.2}Fe_{0.8}O_3$ (LSCF) [47]. LSM and LSCF materials can act as mixed ionic and electronic conductors (MIECs), but, similar to the anode, the electrolyte material is often added to the cathode to improve thermo-mechanical performance. Current is removed from the electrodes using metallic meshes or bipolar plates, normally with the addition of a gasket layer to seal reactant gases to their respective electrodes. Similar to the configuration within a PEFC, the bipolar plates in SOFCs are often etched in order to optimise mass transport. Thermal expansion mismatch remains a prominent source of degradation in SOFCs, the implications of which are primarily observed in the start-up and shut-down times. Therefore, thermal ramp-rates are typically limited to below 5 $^oC\ min^{-1}$ in order to prevent delamination and cracking. Whilst this has been combatted by the addition of ceramic to the anode to reduce undesirable macroscopic thermal expansion arising from mismatch between the constituent layers [48], microscopic interactions in both isothermal [49] and non-isothermal [50] environments are still thought to be problematic. The ceramic skeleton is also thought to impede agglomeration mechanisms in both electrodes [51, 22].

The anode and cathode are often fabricated in the form of functional and support layers whereby the two layers have characteristically fine (1 nm – 1 µm) and coarse (1 µm – 10 µm) feature sizes to respectively promote catalytic activity and mechanical rigidity [52]. Bipolar plates and gasket connections have received less attention in materials research, but the bipolar plates can also cause thermal expansion issues [53] and gasket failure can cause oxidation of the anode [54].

## Microstructures and X-ray Characterisation

### Advancing Electrochemical Device Microstructures

As discussed in the previous sections, electrochemical devices are fabricated with complex microstructures, whereby the particle sizes within the structure and the distribution of the materials are optimised in order to maximize performance, mitigate degradation and delay failure. These structures also often contain graduated structures, where multiple length scales are employed to promote a range of performance advantages at various stages within the cell, i.e. larger structures for mechanical performance, and smaller particles for higher electrochemical activity [55].

It has also been discussed how the numerous materials within the cell can be distinguished and characterised according to their interactions with X-rays. The attenuation,

diffraction and fluorescence of a well-defined monochromatic beam can be predicted for each material within a cell [56], resolved spatially through the use of 3D tomography techniques and resolved with time (4D) by repeatedly examining the same ROI [57]. Example microstructures for a LIB, PEFC and SOFC are displayed in Figure 1, with comparison to a simplified schematic of an electrochemical cell. Significant research has been applied to the pursuit of comprehensive tomographic studies of electrochemical devices and will now be assessed for each device in turn.

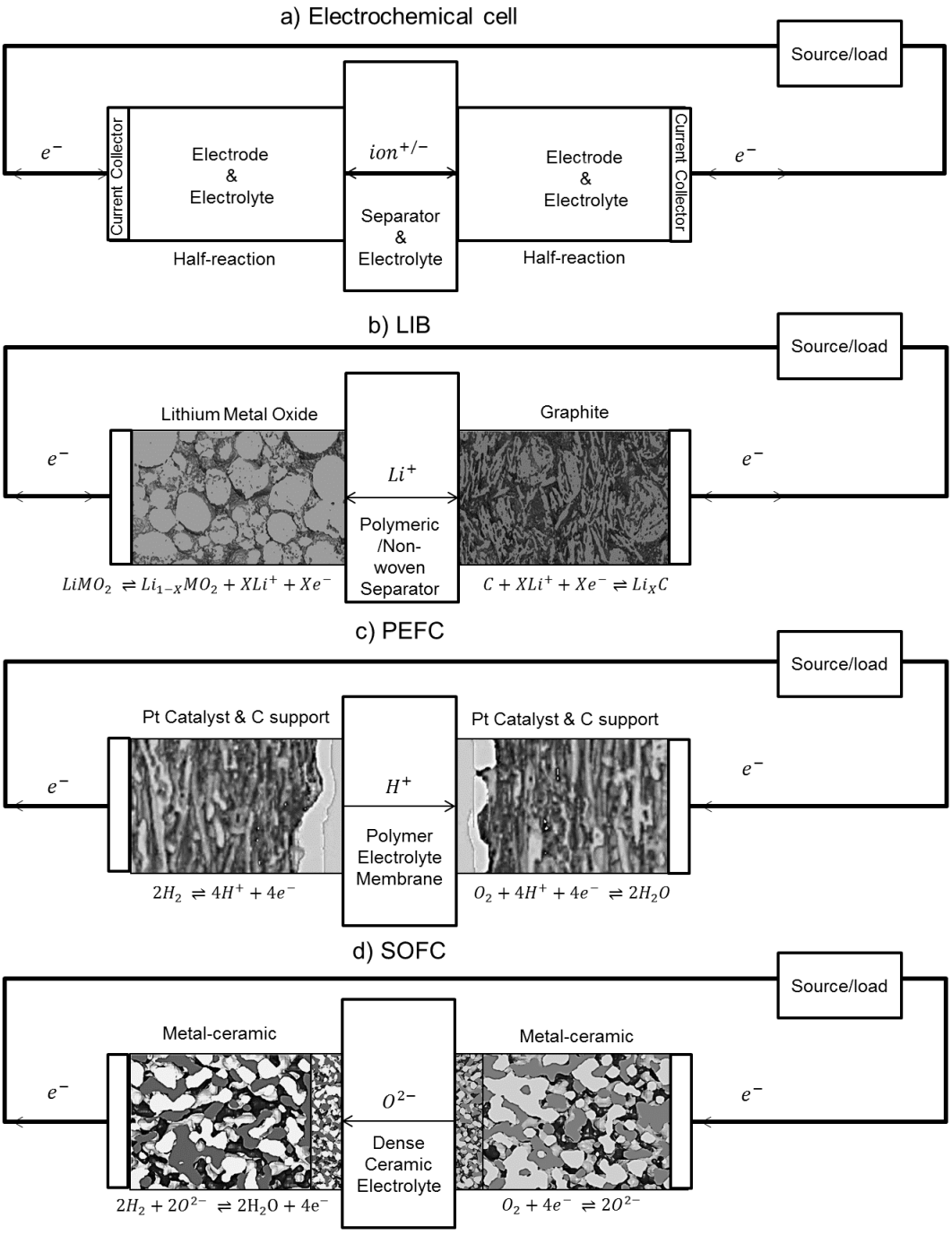


**Figure 1** Four simplified schematics to explain the working principles of a) an electrochemical cell, b) a lithium-ion battery (LIB), c) a polymer electrolyte fuel cell (PEFC), and d) a solid oxide fuel cell (SOFC).

## X-ray Characterisation of LIBs

Early work on the structural characterisation of LIBs was conducted using FIB-SEM [58] and demonstrated the 3D investigations that could be carried out on these microstructures, as well as the useful metrics that can be extracted. Shearing et al. [59] were the first to report the successful reconstruction of a graphite electrode using X-ray tomography. This work pioneered the use of non-destructive tomography in the characterisation of LIB structures. Liu et al. later employed a combination of FIB-SEM and X-ray techniques to characterise lithium cobalt oxide (LCO) and combinations with lithium nickel manganese cobalt oxide (NMC) such as LCO/NMC electrodes [60] concluding that metrics extracted from FIB-SEM and X-ray CT produced comparable results.

It has since been demonstrated that X-ray nano-CT can be used to reconstruct the microstructures of electrodes with multiple active phases (Fig. 2a) [61], even distinguishing and quantifying individual particles [62] and the solid-electrolyte-interface (SEI) [63]. Although capable of differentiating multiple electrode materials, achieving confident distinction of the CBD in 3D with X-ray CT is non-trivial due to its poorly attenuating nature. It is, therefore, common to employ models to generate the CBD. Zielke et al. and Trembacki et al. have demonstrated the use of tomography data in combination with CBD modelling on electrode structures [64, 65]. This was later built upon by Moroni et al., whereby correlative FIB-SEM and X-ray CT were employed to produce reliable tertiary segmentation (Fig. 2b) [66].

Although challenging, reports of successful mappings of the CBD are rising: Daemi et al. demonstrated methods to directly characterise the CBD using lab-based X-ray nano-CT to estimate the ensemble tortuosity factor for LIB positive electrodes [67]; alternatively, Morelly et al. have shown that the use of contrast-enhancing agents such as carbon-coated iron nanoparticles may also prove useful in resolving the CBD [68]; and, Müller et al. have shown that the detachment of the CBD from the active material can be visualised and quantified in order to examine such phenomena with cycling [69].

A key example of the use of three-phase mapping has been demonstrated by Usseglio-Viretta et al. [70] who produced a comprehensive study comparing tortuosity-factor estimation methods for graphite and NMC electrodes. However, the applications of three-phase mapping and quantification are not limited to LIBs: Tan et al. [71, 72] assessed the effective molecular diffusivity of the pore phase and electrical conductivity of the conductive carbon and binder phase via three-phase segmentation in order to conduct simulations of a lithium-sulfur cell.

X-ray phase contrast imaging can be a useful tool in materials characterisation [73]; Babu et al. employed phase and absorption tomography to separate the constituent phases within a LIB structure [74]. Subsequently, Taiwo et al. reported the use of overlaying both phase and absorption techniques to improve image contrast [12]. As displayed in Figure 2c, the data obtained from absorption and phase imaging techniques provides complementary information and, once combined into a single dataset, can produce data with significantly enhanced image quality.

As a result of the non-destructive nature of X-ray characterisation and the scalability of X-ray optics, tomographic methods have been used to investigate LIB structures across multiple length scales [75]. Particularly, the safety implications of cell failures are a prominent focus of LIB research, with Yufit et al. presenting the first use of lab-based X-ray micro-CT for the post-mortem analysis of a failed LIB pouch cell (Fig. 3a) [76]. This has more recently been followed by the work of Robinson et al., in which the failure of lithium and sodium cells were compared using lab-based instruments (Fig. 3b) [77], and work by Chen et al. investigating the swelling failure experienced during low-temperature operation [78].

Cylindrical cells have also been investigated during failure; Finegan et al. conducted high-speed tomography and radiography of 18650 cells during failure achieving 1250 frames per second. This work has been succeeded by a series of investigations combining tomography, radiography and thermography into the dynamics during penetration of the cell [79], internal short-circuits [80] and the causes of cell rupture [81] (Fig. 3c and 3d).

The multi-length scale approach to structural analysis is also important in establishing the degree of homogeneity within the LIB, as heterogeneities may have effects on the

durability of the battery [82]. Cooper et al. reported the characterisation of lithium iron phosphate (LFP) material characterised using X-ray nano-CT and explored the vectorial tortuosity through the sample to expose heterogeneities [83]. Thus, the use of tomography in the examination of non-uniform structures and the possible repercussions of such defects was demonstrated.

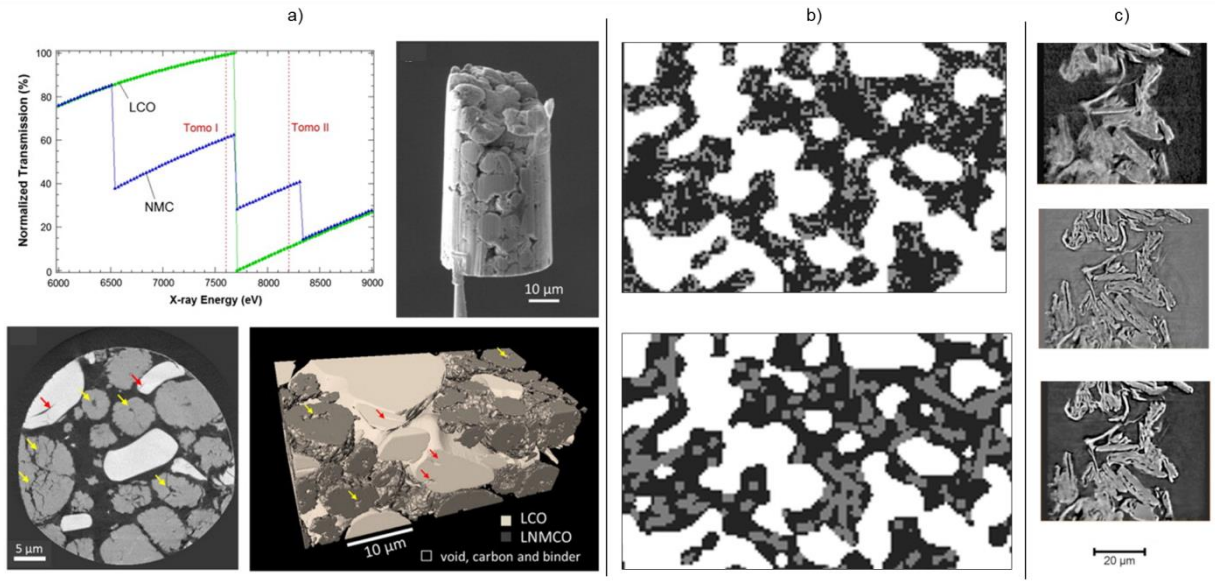


**Figure 2** Electrode-level characterisation of LIBs: a) work by Chen-Wiegart et al. exploring LCO and NMC composite electrode materials, b) CBD generation by Zielke et al. whereby the active material (white) and generated CBD (grey) for two models: random cluster and fibre, and c) the use of combined absorption- and phase-contrast imaging to produced enhanced image quality demonstrated by Taiwo et al. Reproduced with permission of the respective authors [61, 64, 12].

Many degradation mechanisms progress through the evolution of a material over its operating lifetime. Therefore, it is beneficial to collect multiple three-dimensional datasets throughout the aging or failure of the cell. As discussed, macro-scale failure mechanisms are well reported for LIBs, but achieving spatial resolutions capable of capturing micro-scale mechanisms often requires samples that are very small, on the order of tens to hundreds of microns, making repeat analysis very difficult. Chen-Wiegart et al. investigated the oxidation-triggered morphological evolutions within a lithium-vanadium oxide $LiVO_2$ (LVO) electrode using synchrotron radiation [84]. Furthermore, Taiwo et al. conducted an extended cycling study into the degradation of silicon during lithiation using operando synchrotron X-ray CT [85]; and, Tsai et al. demonstrated the use of X-ray characterisation to conduct single particle measurements [86]. Moreover, Villevieille et al. harnessed both XRD and X-ray CT for operando investigations into the lithiation of single particles [87]. However, the availability of synchrotron radiation is limited, so the advancement of lab-based instruments has increased the possibilities of extended duration studies. Recently, Heenan et al. reported the use of a 4D X-ray nano-CT sample preparation and mounting technique compatible with a diverse range of applications from the lab to the synchrotron that is stable within a range of environments, including high temperature and gas environment studies [88].

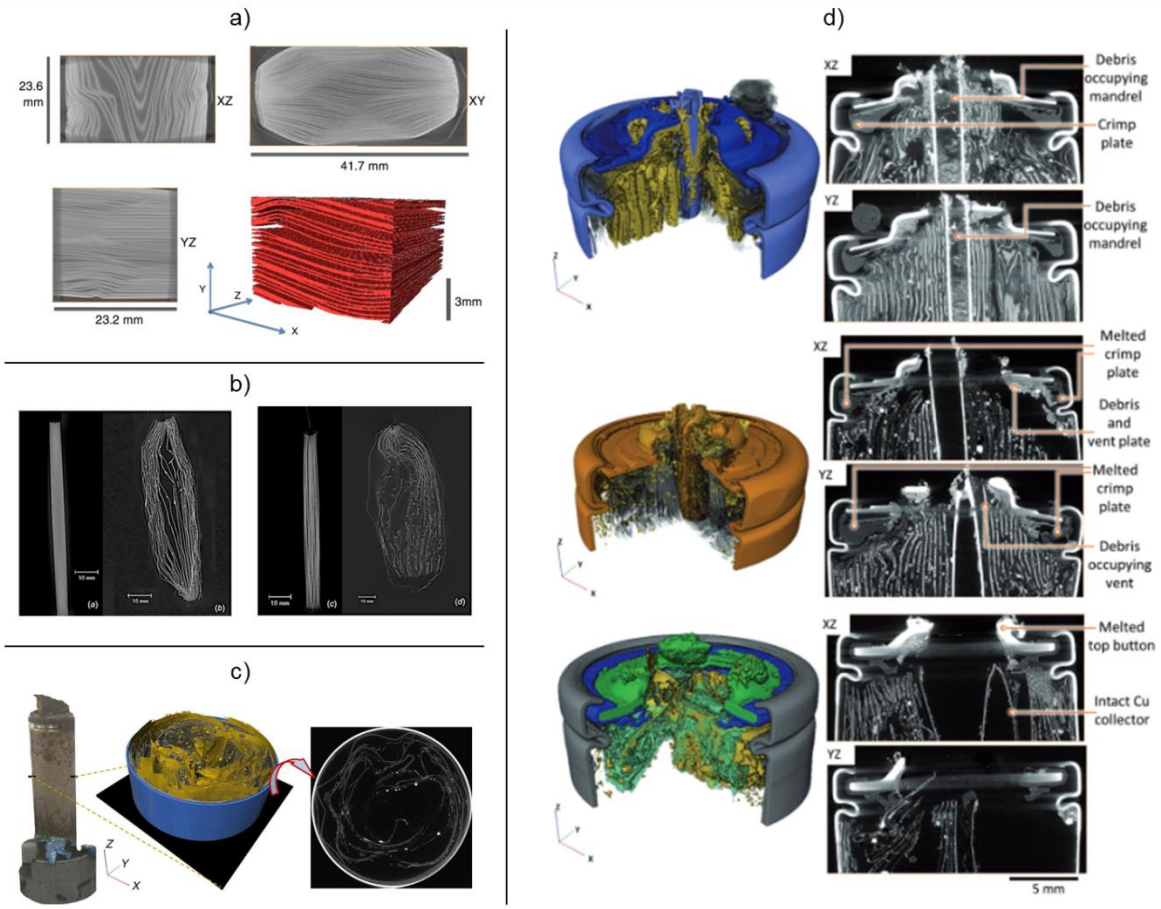


**Figure 3** Cell-level characterisation of LIBs: a) Cross-sections from a failed LIB pouch cell characterised by Yufit et al., b) a comparison of the failure of sodium and lithium pouch cells by Robinson et al., c) failure of an 18650 cylindrical cell captured with high-speed CT, d) failure for three cell types: Sanyo (top), Panasonic (middle), and Samsung (bottom). Reproduced with permission of the respective authors [76, 77; 81].

The cell designs for in situ and operando studies are continuously evolving with designs often produced that are specific to an instrument or beamline. Tan et al. [89] concisely summarises the current state of the literature on cell designs including material choice and the subsequent benefit and drawbacks. The nature of “four-dimensional” data allows for the additional analysis through computational methods such as digital volume correlation (DVC), whereby 3D datasets obtained from the same region of interest can be directly compared in order to track the movement of individual features in the production of displacement vectors. Figure 4a is reproduced from work by Paz-Garcia et al., which visually describes the computational methods employed in DVC [90]. Leung et al. along with Luo et al. employed such methods on data obtained from real-time displacements at the cell-level of a pouch LIB during the charge-discharge process [91, 92]. DVC has also been used to explore the bulk electrode strain and material displacement within an 18650 cell during failure [93]. Eastwood et al. used DVC to investigate the lithiation-induced dilation within a LIB coin-cell (Fig. 4b) [94], whereby the displacement vectors of the individual grain were quantified i.e. particle-level characterisation. Silicon is a popular candidate for the addition to, or replacement of, graphite electrodes due to its high energy density; however, silicon particles are known to experience large volume changes during lithiation, which has made them a prime candidate for DVC studies [90, 95]. More recently, Daemi et al. have employed the use of 4D analysis to mimic the early stages of calendering, a method often applied to LIB electrodes in order to improve

the packing density, thus volumetric energy density. Their work showed novelty in the use of a compression stage to achieve in situ characterisation [96].

Image-based modelling can provide a powerful tool in the prediction and optimisation of LIBs [83]; as previously mentioned, models based on X-ray CT data may be employed to generate structures or evaluate local transport properties [70], allowing 3D or 4D distributions of local current or potential to be mapped [97], possibly even across multiple length scales [98], even to the extent of cell failure [95]. Nevertheless, imaged-based modelling such as this is not limited to LIB and has recently seen interest from other battery chemistries [71, 99].

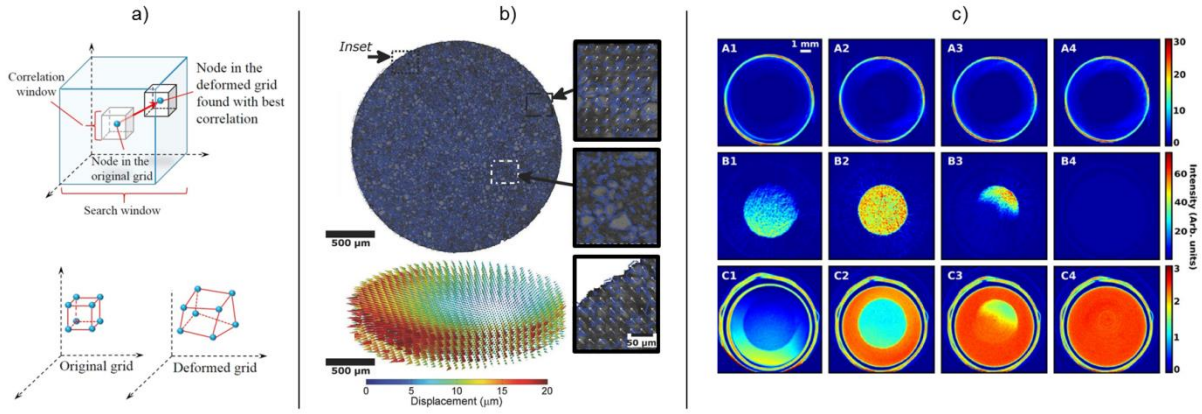


**Figure 4** Advanced characterisation methods: a) schematic representation of digital volume correlation (DVC) methods as described by Paz-Garcia et al., b) DVC in practice, applied to a LIB cathode observing morphological changes during de/lithiation, and c) the application of X-ray diffraction tomography demonstrated by Jensen et al. on a LIB coin cell. Reproduced with permission of the respective authors [90, 94, 100]

X-ray tomographic methods are not limited to reconstructions based upon attenuation information; diffraction patterns can provide additional information about the structure, composition, strain and stress, and X-ray diffraction computed tomography (XRD-CT) can be a powerful tool in the characterisation of crystalline materials, as discussed by Jensen et al. (Fig. 4c) [100]. Moreover, diffraction-based imaging is, theoretically, not limited to the precision of the instruments during manufacture i.e. the zone plate design and can therefore approach spatial resolutions near the wavelength of the incident X-ray, as discussed by Hitchcock et al. [101]. Coherent Diffraction imaging (CDI) can expose detail at extremely high spatial resolutions as demonstrated in the form of operando dislocation imaging by Ulvestad et al. [102]; however, obtaining information within an operating cell is extremely challenging due to demanding sample requirements. Furthermore, the use of ptychographic methods allowing chemical states to be resolved in 3D as demonstrated by Yu et al. with nanometre resolution [103]. The use of such powerful tomographic crystallography techniques is expected to rise in coming years and will be discussed further in the perspective and outlook section.

X-ray Characterisation of PEFCs

Earlier work on PEFC characterisation using X-ray CT was carried out by Sinha et al. [104], who demonstrated the use of lab-based X-ray micro-CT to quantify liquid water distributions within a PEFC using a ca. 10 µm voxel size. Their work explored the water saturation within the GDL, which is critical in optimising cell performance. However, resolving the structure of the carbon fibres with spatial resolutions around ca. 10 µm or larger can be problematic. Therefore, later studies by Krüger et al. employed the use of synchrotron radiation to achieve a voxel size of under ca. 5 µm. Thus, the influence of flow field design on the cell structure and the relationship between hydration and current density could be inspected [105]. Flückiger et al. carried out similar synchrotron experiments but with the use of multiple resolutions, as

low as sub-micron, thus allowing for resolution of fibre features in the GDL. Their work also employed a mixture of absorption and phase contrast imaging, which allowed weakly attenuating features to be enhanced, at some expense of temporal resolution during phase contrast acquisition. The wide range of imaging parameters used allowed for a thorough analysis of liquid water distribution in the GDL in 1-, 2- and 3D, including insight into the inhomogeneous way in which water fills the pores in the GDL [106].

Since the layers of the MEA comprise features spanning the length scales, from the micron-sized fibres of the GDL to the nano-pores of the CL, X-ray CT is a particularly well suited technique for imaging across these length scales. Adopting a multi-scale approach to imaging, the X-ray CT instrument chosen can elucidate different features of the PEFC, such as the studies by Meyer et al. [107] and Normile et al. [108]. At the nanoscale, Epting et al. continued the pursuit of high spatial resolution imaging, achieving X-ray nano-CT without the use of synchrotron radiation [109]. Their work explored the solid and porous structures within two electrodes prepared with different size agglomerates using a resolution of 50 nm as seen in Figure 5. Furthermore, comparison to the experimental metrics obtained with mercury intrusion porosimetry validated that X-ray CT produced comparable results for pore sizes larger than 50 nm. Further work from the same group saw Lister et al. conduct X-ray nano-CT using lab-based instruments to study variable temperature Knudsen diffusion and its comparison to experimental data. Again a close agreement with the X-ray CT data was found [110]. Since platinum-group free metal catalysts are a particular research focus for PEFCs, work by Babu et al. highlighted the suitability of X-ray nano-CT for elucidating transport properties, including diffusivity and conductivity, in novel non-Pt-containing cathode catalyst layers [111].

For in situ or operando investigations of PEFCs, specialised cell designs must be developed, such that a representative volume of, generally, the MEA with flow fields can be imaged on a suitable timescale for capturing the processes of interest, such as water distribution. The need to understand water-phase transport properties is crucial for PEFCs; flooding of the materials in the MEA has a significant detrimental effect on cell performance. Owing to the high temporal resolution of synchrotron X-ray CT, a significant amount of the research has been carried out at facilities worldwide. James et al. demonstrated a system for the investigation of heterogeneous compression effects on the GDL as seen in Figure 5b. Their studies found that transport of species performs best in the direction in line with the fibres and that the compression of fibres can result in transport properties differing by a factor of two between the land and channel regions [112]. Gaiselmann et al. later built upon this through the development of models describing fibres under compression [113]. Combined imaging and pore network modelling of the 3D datasets allowed Fazeli et al. to predict the water distribution in various compressed GDLs [114]. Work by Lee et al. focused instead on various thicknesses of MPL and it was found that a thicker MPL aided water management by reducing accumulation of water in the interfaces within the GDE [115]. Zenyuk observed water distribution in the GDL in situ, with the addition of land and channel compression effects through various compression levels, achieving the segmentation of spatially resolved water distributions (Fig. 5c) [116]. Other operando studies of water distributions in PEFCs have included work done by Alrwashdeh to quantify the water in the pores of the MPL in the MEA [117]. By subtracting images of the dry and operating cell, the water content could be quantified to highlight the location of water accumulation in the pores. Another operando investigation of the liquid water properties in a PEFC run at 80 °C was demonstrated by Eller et al. [118]. An in-depth analysis of the water distribution in the cell allowed for properties like saturation, connectivity and permeability of water to be quantified. Cold-start is one of the engineering challenges for PEFC design; in cold climates, fuel cell vehicles could be required to start-up at below-zero temperatures. To understand the effects of freezing on operating fuel cells, fast tomography studies were carried out on freeze-started PEFCs [119]. With a total scan time of 4.9 s, the evolution of water between -10 and -20 °C was investigated. Performance drops over the start-up could be attributed to three different freezing mechanisms, which varied according to the temperature and current density of the cell.

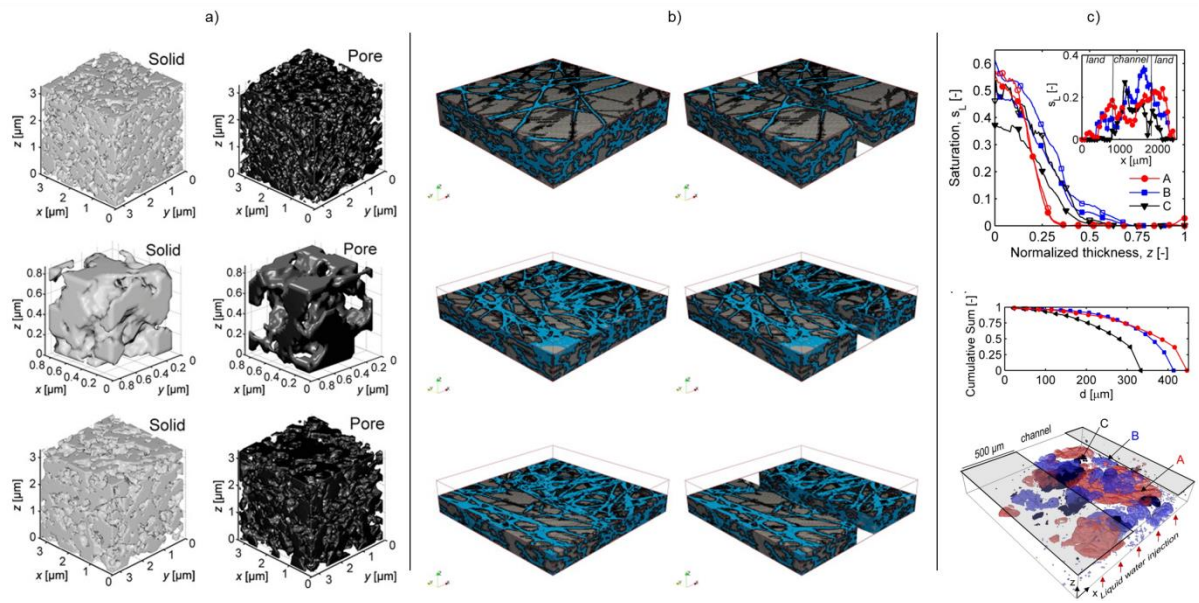


**Figure 5** Polymer electrolyte fuel cell characterisation; a) electrode-level segmentation of solid and pore phases by Epting et al., b) cell-level characterisation by James et al. of the effects of compression with segmented solid (blue) and porous phases (grey), and c) investigations by Zenyuk et al. into the liquid saturation as a function of normalized GDL thickness. Reproduced with permission of the respective authors. [109, 112, 116].

Since the ionomer additive in the GDEs is particularly susceptible to damage by X-ray irradiation, when exposed to the intense X-ray beam a drop in performance of operando cells can occur, as observed by Eller et al. [120]. The performance drop was attributed to two main degradation pathways arising from X-ray irradiation: an irreversible reduction in water contact angle resulting in flooding of the CL and a partly-reversible poisoning of the CL with sulfate species formed from degradation of the ionomer. In contrast to the findings of Eller et al., White et al. did not see an appreciable degradation of fuel cell performance in an operating cell when using a lab-based source [121]. This suggests that the high brilliance of the synchrotron beam has a more significant effect on the operation of PEFCs. Thus, careful selection of imaging parameters, with minimal possible beam dose, is crucial for avoiding artefacts arising from the X-ray beam.

The use of X-ray CT for PEFCs has also been invaluable for the inspection of variations within the manufacturing of MEA components. Odaya et al. quantified the porosity distributions within single layer GDLs from different manufacturers, attributing heterogeneities to the ply manufacturing process, the preferential agglomerating of binder and PTFE, and the drying procedure [122]. Felt-type and paper-type GDL materials were compared by Banerjee et al., with X-ray CT providing information about the 3D microstructure of the various materials, and X-ray radiography shedding light on the water accumulation across the cell [123]. The effect of GDL material on water transport was investigated by Jinuntuya et al. using Lattice Boltzmann methods [124]. Continuing the inspection of MEA fabrication methods, Meyer et al. studied the hot pressing process for various temperatures observing considerable differences in cell structure and properties (Fig. 6) [125]. Image-based modelling is an invaluable technique for understanding pore-scale transport dynamics in PEFCs, especially in the GDLs, where two-phase flow, i.e. water and gases, is common. Thus, the combination of actual X-ray CT datasets with modelling studies has allowed for a deepened understanding of these transport properties; now modellers can build their computations based upon real materials, rather than randomly generated simulations [126]. Hinebaugh et al. carried out some of the first of these studies by employing a 2D pore-network model based on X-ray CT datasets of various GDL materials [127, 128]. Their findings showed that GDLs are more liable to localised flooding when the porosity distributions of the carbon papers have many so-called “peaks and

valleys", i.e. a local maxima in the porosity distribution correlated strongly with a highly saturated area in the GDL. Work by Hasanpour et al. used commercial GDL samples to compare the flow of reactant species through the pores in the fibre- and MPL-phase [129]. García-Salaberri et al. also demonstrated the use of modelling, to understand the effective diffusivity in GDLs with varying PTFE content and saturation levels [130]. A micro-CT dataset of a dry GDL was used by Sabharwal et al. to build a full morphology model, which simulated liquid water intrusion into the GDL. Results of the simulation showed good agreement with experimentally obtained wet GDL datasets, highlighting that the model constructed was efficient at predicting liquid water saturation in the GDL [131]. Other demonstrations of image-base modelling have included a number of studies using X-ray CT datasets to understand water evaporation in GDLs [132,133].

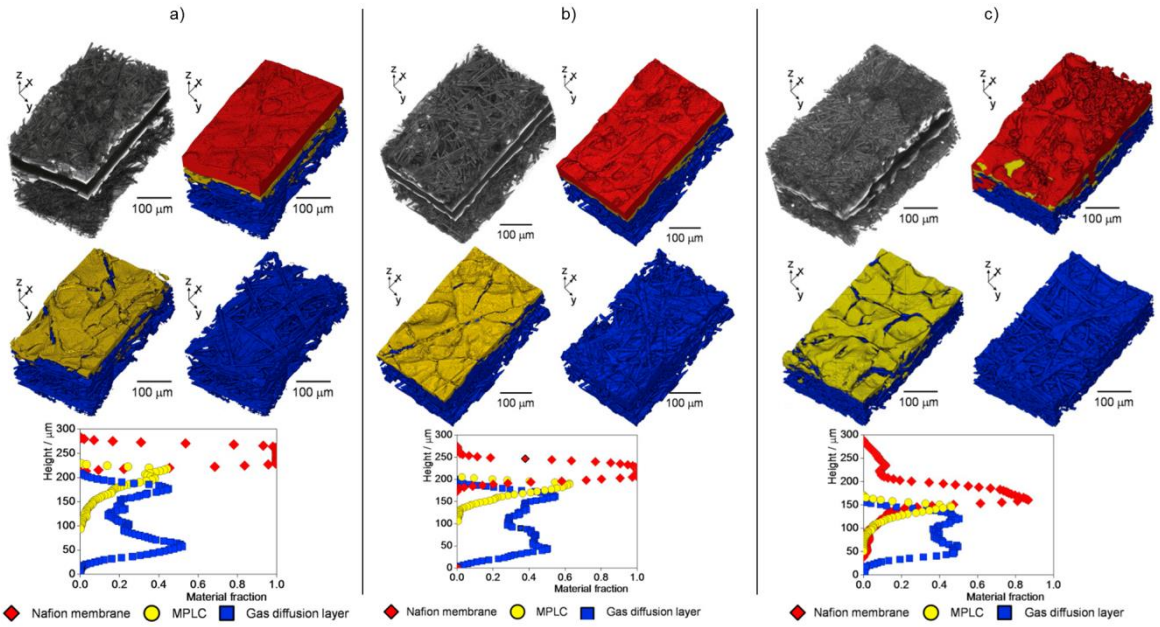


**Figure 6** Investigation in the effects of hot pressing temperature on PEFCs carried out by Meyer et al., where the cell microstructures are investigated after pressing at three temperatures: a) 100 ºC, b) 130 ºC, c) 170 ºC. Reproduced with permission of the authors [125].

As well as 'beginning-of-life' investigations, the MEA microstructure at the end of life is also of interest; there is a need to further understand the intricate mechanisms that are responsible for degradation and failure of PEFCs. Hack et al. carried out work investigating methods for MEA fabrication [134]. Through the comparison of hot pressed and self-assembled cells, the microstructures and electrochemical performances at both the beginning and end of life were investigated. Other work into MEA degradation has seen the examination of CL degradation across multiple length scales, including the observation of crack propagation, CL thinning and porosity reductions [135]. Membrane degradation was also studied using X-ray CT, and the reduction in electrochemical performance pertaining to the membrane could be correlated to increased cracking of the membrane [136]. More recently, periodic electrochemical diagnostics in combination with lab-based X-ray CT imaging was used to characterise degradation in 4D by White et al. [137]. Their work observed variations in the degradation of land and channel regions, with crack formation and propagation within the cathode catalyst layer. Crack propagation in the membrane could also studied using 4D, time-resolved studies by Singh et al. [138]. Further work from the group allowed for a joint visualisation approach, imaging both CL degradation and liquid water accumulation [139]. This allowed for a rigorous analysis of changes in the CL during degradation, such as variation in pore structure and loss

of carbon support, whilst understanding more about the flooding of liquid water in both the nano-pores of the CL and the micro-pores of the GDL.

X-ray Computed Laminography (XCL) [140, 141] has also proven to be a useful method of analysis; Saida et al. [142] demonstrated the use of XCL in combination with X-ray Absorption Fine Structure (XAFS) [143] in the form of Laminography -XAFS to examine the cathode CL in 4D exposing Pt distribution before and after degradation. XAFS has also been demonstrated operando by Ozawa et al. [144] who utilised this technique to explore the rate of Pt-O bond formation with potential. Recently, Yu et al. demonstrated the use of Hard X-ray Photoelectron Spectroscopy (HAXPES) in order to examine sulphur poisoning of such Pt CLs [145]. The developments of the Spring-8 BL36XU beamline where such operando experiments can be undertaken has been summarised elsewhere [146].

## X-ray Characterisation of SOFCs

The first 3D reconstruction of an SOFC anode was accomplished by Wilson et al. using a FIB-SEM reconstruction [147]. Shortly afterward, Izzo et al. produced a 3D reconstruction using X-ray CT with sub-50 nm resolution [148]. As with other highly attenuating materials, small sample sizes are required for the reconstruction of high spatial resolution datasets. Early work by Shearing et al. established a reproducible method for sample preparation using FIB milling of a sample from the material bulk followed by welding to a pin head [14]. This has since been used extensively for a variety of materials characterisation using X-ray CT. The difference between FIB-SEM and X-ray CT characterisation has been compared for both anodes [149] and cathodes [150, 151], and comparable results have been observed between the two techniques.

The TPB reaction sites within the SOFC are of particular interest due to the inherent link between their population density and the performance of the cell. Guan et al. investigated the TPB using synchrotron radiation and the volume required in order to achieve statistical representation [152]. Laurencin et al. later built upon the work demonstrated by Wilson et al. by exploring prominent metrics such as the pore tortuosity, which is critical in optimising the gas diffusion processes, using significantly larger sample volumes via X-ray CT [153]. While metrics like the TPB density and tortuosity give an indication of the electrode performance at the time of measurement, these metrics are known to change during operation as a result of microstructural degradation mechanisms. Nelson et al. explored the microstructural changes associated within the Ni-YSZ electrode during operation through the analysis of samples taken at several points in the cell lifetime. Although this study was not completed on the same region of interest, i.e. new samples were collected for each X-ray CT analysis, consistent trends were observed in the results: the mean Ni particle diameter increases with time (Fig. 7a) [154]. Kennouche et al. expanded this analysis exploring the changes associated with the reaction sites with temperature and time; the TPB density and Ni-YSZ contact area were both found to decrease with increasing operation time (Fig. 7b) [155]. Chen-Wiegart et al. then followed these studies by analysing the effects of the Ni content on the morphological evolution of the Ni-YSZ structure with operational cycling [156].

Two other prominent mechanisms for SOFC degradation are redox cycling and poisoning of the metal. Shearing et al. inspected the anode structure with sequentially increasing temperature elevations, exposing intricate oxidation mechanisms that are responsible for Ni migration [157]. Following this, Harris et al. found that exposure of Ni-YSZ to sulfur poisoning conditions resulted in structural features analogous to those witnessed during oxidation. This study employed 3D nano-probe tomography to combine absorption and XRF imaging for a complementary analysis [158]. Both investigations witnessed internal pore formation within the metal particles indicating analogies between the different forms of chemical film growth (Fig. 8).

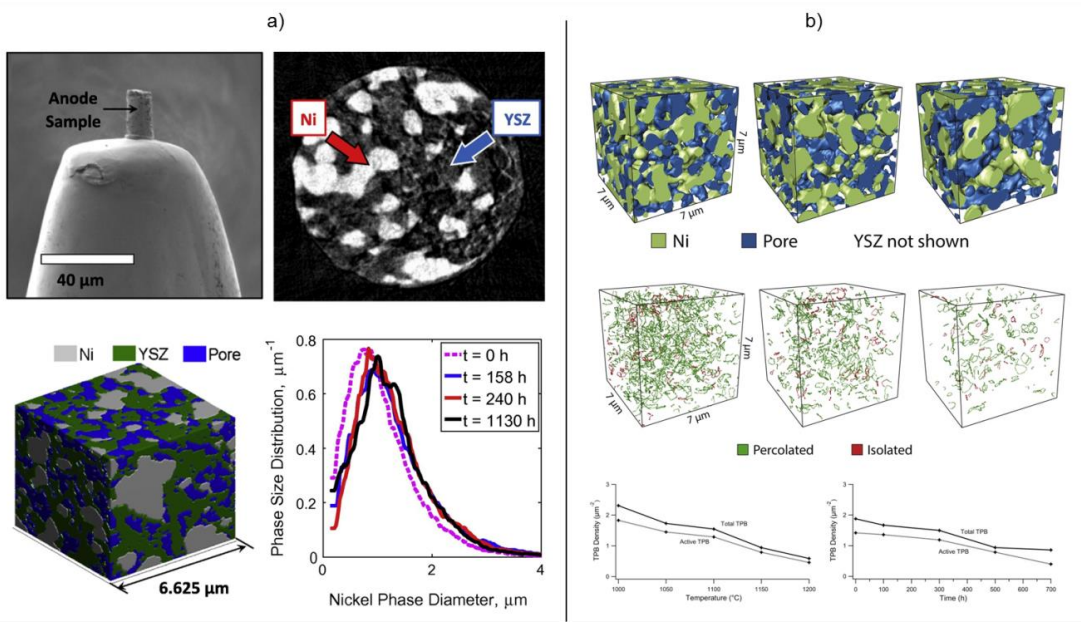


**Figure 7** X-ray nano-CT of solid oxide fuel cell structures: a) FIB milling preparation and subsequent characterisation and segmentation by Nelson et al., and b) functional layer degradation investigated by Kennouche et al. after 50 hours of ageing at 1000 ºC (left), 1100 ºC (centre) and 1200 ºC (right), with TPB maps from structures after 500 hours of ageing at 1000 ºC (left), 1100 ºC (centre) and 1200 ºC (right). Reproduced with permission of the respective authors [154,155].

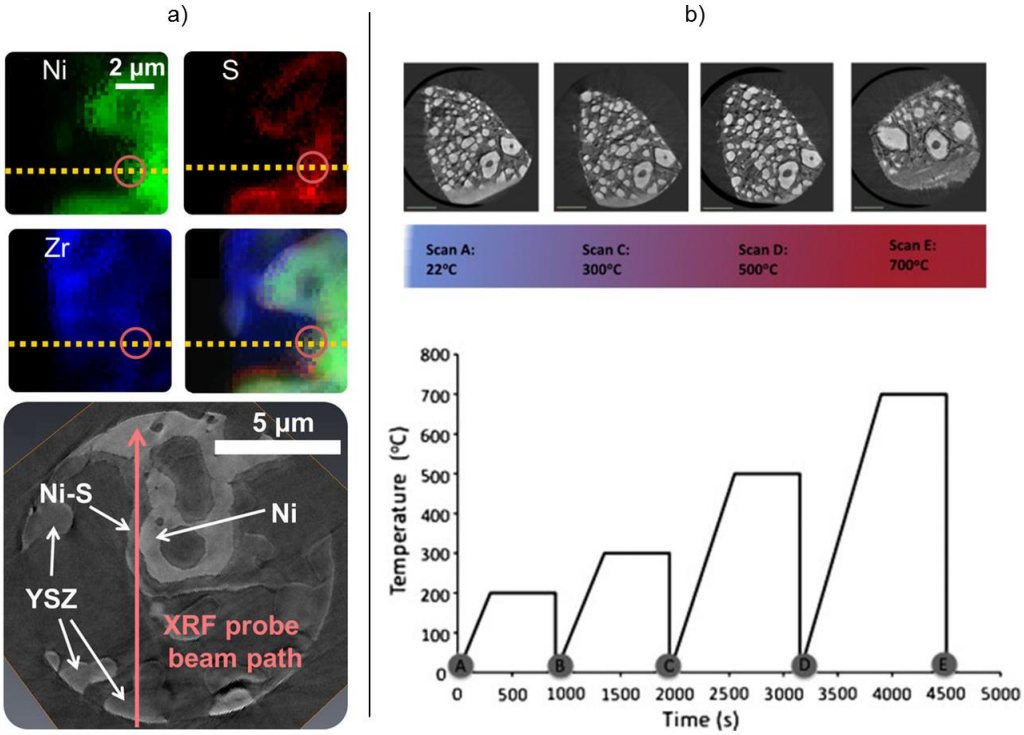


**Figure 8** Advanced characterisation of SOFC materials: a) X-ray fluorescence imaging of a Ni-YSZ electrode poisoned by sulfur imaged by Harris et al., and b) investigations by Shearing et al. into the microstructural changes associated with Ni-YSZ oxidation and the effects of temperature. Reproduced with permission of the respective authors [158, 157].

Although substantial characterisation of the TPB sites had been accomplished using synchrotron radiation, only after significant advancements in lab-based instruments was it possible for non-destructive TPB characterisation to be achieved without the use of a synchrotron. Heenan et al. reported the first three-phase segmentation of SOFC anode materials using lab-based X-ray nano-CT [159]. Since then a wealth of studies have been accomplished from the use of morphological computations on X-ray CT data to investigate the effects of Ni densification on the TPB density [160], to the investigation of phase tortuosity and its impact on mass flux [161, 162] (Fig. 9).

In combination with the aforementioned laser preparation technique [15], Heenan et al. developed a mounting technique [88] whereby samples of desirable sizes can be produced, which are consistently robust even in the extreme conditions of SOFC operation [163, 164]. This has allowed 4D studies to be carried out using lab-based instruments with sub-micron resolution observing mechanisms triggered by operationally relevant conditions [165].

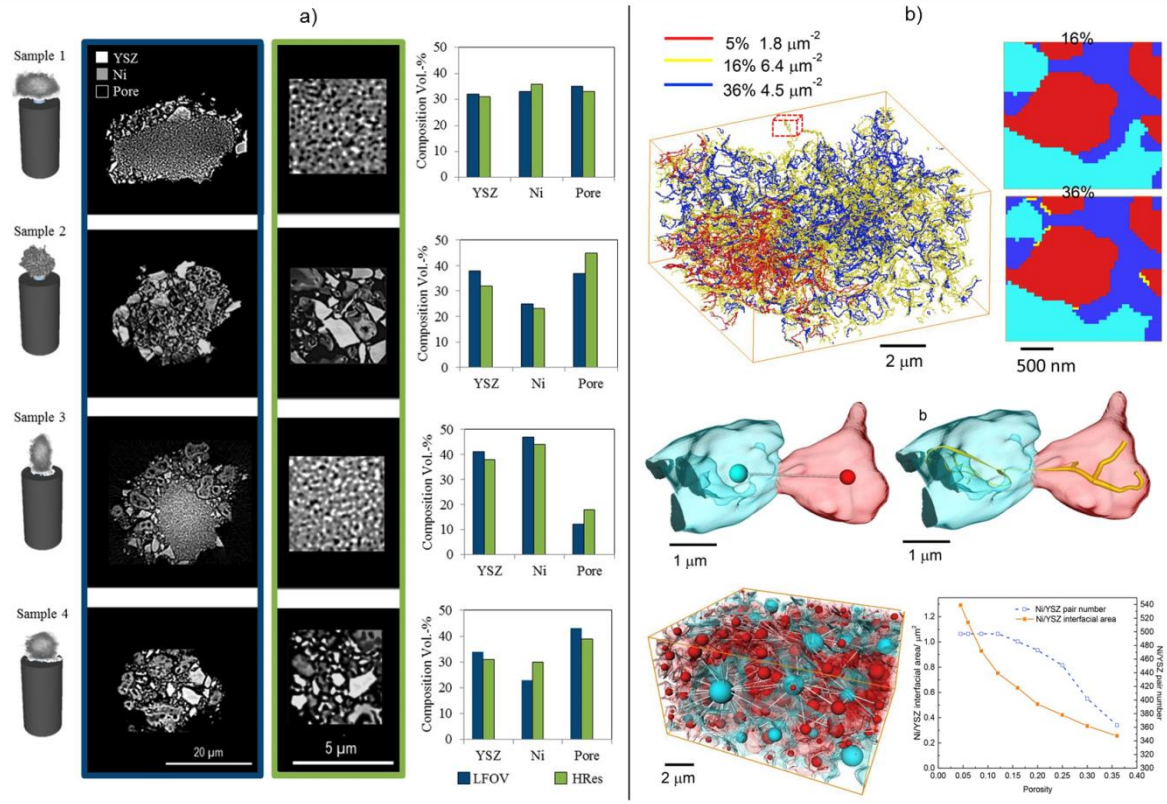


**Figure 9** Lab-based characterisation of SOFC structures: a) three-phase segmentation of various electrode structures with accompanying compositions established by Heenan et al., and various quantifications carried out on SOFC microstructures obtained through X-ray CT by Lu et al. which explore the optimisation of the TPB networks. Reproduced with permission of the respective authors [159, 160].

Finally, similar to the work conducted on PEFCs, modelling across multiple length scales can also be a powerful tool for the investigations of SOFCs. For instance, gas transport modelling can be applied to various structures and geometries [166, 167] and may even be applied to real structures obtained from X-ray CT [168]. Grew et al. concisely review multiscale modelling for SOFCs [169].

# Perspective and Outlook

## Current Perspective

In order for a wide range of electrochemical devices to become commercially competitive, advancements must be made in the fabrication of materials that perform safely and efficaciously for sufficient durations. The intrinsic link between the cell microstructure and the electrochemical performance makes both the initial cell design and the subsequent structural evolutions critical in performance optimisation. Therefore, improved understanding of the effectiveness of fabrication methods in producing ideal structures, as well as the mechanisms responsible for performance losses during operation, is required.

To better understand cell structures in 3D, X-ray CT has become widely employed in capturing structures across multiple length scales. Moreover, the non-destructive nature of X-rays has resulted in the development of many time-resolved studies tracking operationally relevant degradation mechanisms. X-ray characterisation has been employed primarily using absorption X-ray CT; however, phase information has been used to enhance images of inherently intricate structures; fluorescence CT has been employed where chemical changes are of particular interest and, finally, diffraction CT has been utilised to spatially resolve crystallographic information.

Progressing from traditional CT methods, advanced techniques are rapidly emerging as potential tools for cell characterisation: ptychography [170, 171], pair distribution function (PDF-CT) [172], small angle X-ray scattering (SAXS-CT) and XRD-CT [173, 174] each offer unique information capable of building a more complete description of the cell constituents, potentially capable of extending beyond 4D.

When X-ray tomography was initially being employed for investigations into electrochemical devices, synchrotron radiation was typically required. However, recent advancements in lab-based instruments have resulted in the achievement of comparable spatial resolutions without the need for specialist synchrotron facilities. Despite this, the beam brilliance achievable with lab-based instruments remain orders of magnitude lower, resulting in significantly longer acquisition times, e.g. lab-based nano X-ray CT may be on the order of hours whereas the synchrotron may be on the order of minutes. Additionally, the monochromaticity of X-ray tubes remains inferior to that of synchrotron radiation and often results in limited variability in the source energy, as well as difficulty in the removal of undesirable Bremsstrahlung radiation.

## Future of Batteries

The future of X-ray CT characterisation of batteries may look to advance away from attenuation-based CT: X-ray diffraction can provide additional information about the structure, composition, strain and stress, and as beamline instruments improve, the capabilities and application of such techniques in the study of structures in situ and operando is expected to increase. For instance, it is conceivable that diffraction-based CT methods may be employed to inspect the internal crystallography of an operating commercial cell such as an 18650 or 21700 without the need for disassembly. This has, as of yet, been challenging due to the introduction of parallax error [175]; although, improved reconstruction algorithms may overcome this, allowing the investigator to explore the spatially resolved temperature and strain distribution through the windings of the cell during operation. Mechanisms that are of particular interest during operation may form the focus of several future studies, e.g. gas evolution [176, 177, 178]. Moreover, with the ever improving beam precision, pixel sizes in the tens of nanometres would make it plausible for ultra-high resolution, spatially-resolved information to be obtained from single particles, similar to that which has been presented by Tsai et al. [86], with the added benefit of crystal mapping if conducted using a diffraction detector, and/or oxidation state mapping if conducted around an X-ray edge. And finally, if the aforementioned techniques are employed within a bespoke cell housing, as discussed by Tan

et al. [89], the crystallography and/or oxidation states can be correlated to the electrochemistry [179], providing the opportunity for highly comprehensive correlative studies.

### Future of PEFC

For PEFCs, the limitations in the spatial resolution of X-ray CT has restricted the number of studies on the nano-scale features of the CL; investigations have widely been constrained to ex-situ TEM studies, which do not capture the CL in its operating environment, i.e. within the MEA. Of the few examples of nano-scale studies conducted with X-ray CT, most do not allow for imaging of individual particles or clusters of platinum. However, with the continuing improvements in resolution of X-ray CT instruments, it is conceivable that in situ or operando studies of nano-scale features could be achieved. Furthermore, the development of other tomography techniques, such as spectroscopic scanning coherent diffraction imaging (spectro-ptychography) [180] or X-ray absorption near edge structure (XANES) [181], have started to allow such studies on the CL. By tuning the beam energy to the various electron shell edges in the materials of interest, 3D elemental maps can be created. Hence, such techniques unlock new possibilities for studying degradation mechanisms relevant to the CL, such as platinum agglomeration or dissolution into the membrane. Finally, with the continuous decrease in acquisition times of both lab and synchrotron sources, many more possibilities for time-resolved studies are unlocked. This could be anything from understanding the drying process during catalyst spraying, to the degradation of MEA components over time, to increasing the volume of sample imaged, improving statistical significance of acquired datasets.

### Future of SOFCs

Apart from the few reports discussed here, the literature on the operation and degradation of SOFCs in 4D remains limited. Furthermore, the materials that have been investigated by methods such as X-ray CT are also restricted typically to the anode, specifically Ni-YSZ. However, issues with, for instance, the cathode current collection may also provide valuable insight into performance loss if evaluated in 4D. Furthermore, many chemistries are emerging as next-generation electrode materials such as mixed-ionic-electronic-conductors (MIECs) [182], which may also benefit from such studies. Finally, there are many possibilities for employing XRD-CT to investigate SOFC materials; although investigations using point- and powder-XRD into SOFCs, particularly with focus on the anode [49, 50], have proven very valuable, extending such studies to become spatially resolved would further elucidate the origins and developments of cell constituents. For example, the ability to spatially resolve the multi-scale, structural, chemical and mechanical developments through temporally and spatially resolved crystal-, nano-, micro- and macro-structural mapping can provide unprecedented insight [183].

### General Outlook

Looking forward, the advancement of readily-accessible, lab-based instruments will result in a greater quantity of studies being possible, improving the statistics on the data obtained and deepening the understanding of materials within the electrochemical devices discussed here.

Considering the rate of development over the last few decades it is clear that the most valuable studies will strive to progress in the direction of temporally and spatially resolved information that captures structural and chemical information across multiple length scales, all collected operando, under conditions relevant to commercial applications. With the increased undertaking of studies that employ an in situ or operando set-up, factors such as damage due to dosage from the characterising probe i.e. electron, X-ray, neutron, etc., may also become increasingly important and require further evaluation [184, 185]. Achieving operational conditions during characterisation is challenging, but achievable, through the assembly of

bespoke environments [89, 146, 183]. Furthermore, the continued development of synchrotron facilities [186] will result in beams of greater brilliance, improving data quality and reducing acquisition times. This would inevitably lead to the collection of larger, more comprehensive datasets and data handling would become increasingly more demanding; the storage, processing and dissemination of data is often a bottleneck for high-rate tomography, a short experiment of only a few days can result in terabytes of raw data that can increase to tens of terabytes after processing. After synchrotron upgrades, it is conceivable that data output may increase by orders of magnitude. Although potentially challenging to manage, the increased amounts of data may also bring improved statistics that could allow emerging fields such as artificial intelligence (AI) to improve via machine and deep learning algorithms [187, 188]. It is also conceivable that in order to streamline the processing of data, an increase may be seen in the release of open-source and commercial data-processing packages.

Ultimately, the correlative use of various tomography methods in combination with real electrochemical data and models will improve the understanding of the routes to performance optimisation, as well as the necessities to retain that performance over of the course of the cell lifetime. This will, ultimately, aid the development of the next generation of electrochemical devices.

## Acknowledgements

The authors would like to acknowledge the EPSRC (EP/M014045/1, EP/R020973/1), the Centres for Doctoral Training (EP/L015749/1) and (EP/LO15277/1), and the Royal Academy for Engineering (CiET1718\59) for financial support. This work was supported by the Faraday Institution made available through grants EP/R042012/1 and EP/R042063/1.

# Abbreviations

| | |
|---|---|
| Lithium-ion battery | LIB |
| Polymer electrolyte fuel cell | PEFC |
| Solid oxide fuel cell | SOFC |
| Focused-ion beam | FIB |
| Scanning electron microscope | SEM |
| Computed tomography | CT |
| Field of view | FOV |
| Region of interest | ROI |
| X-ray diffraction | XRD |
| X-ray fluorescence | XRF |
| Digital volume correlation | DVC |
| Triple-phase boundary | TPB |
| Carbon-binder domain | CBD |
| Ethylene carbonate | EC |
| Dimethyl carbonate | DMC |
| Diethyl carbonate | DEC |
| Ethyl-methyl carbonate | EMC |
| Polytetrafluoroethylene acid | PTFE |
| Membrane electrode assembly | MEA |
| Gas diffusion electrode | GDE |
| Catalyst layer | CL |
| Microporous layer | MPL |
| Gas diffusion layer | GDL |
| Yttria-stabilised zirconia | YSZ |
| Gadolinium doped ceria | GDC |
| Lanthanum strontium manganite | LSM |
| Lanthanum strontium cobalt ferrite | LSCF |
| Mixed ion-electronic conductor | MIEC |
| Lithium-Vanadium Oxide $LiVO_2$ | LVO |
| Lithium cobalt oxide | LCO |
| Lithium nickel manganese cobalt oxide | NMC |
| Lithium iron phosphate | LFP |

# References


1. Barbir, F., 2006. PEM fuel cells. In Fuel Cell Technology, Springer, London.
2. Singhal, S.C. and Kendall, K. eds., 2003. High-temperature solid oxide fuel cells: fundamentals, design and applications. Elsevier.
3. Nazri, G.A. and Pistoia, G. eds., 2008. Lithium batteries: science and technology. Springer Science & Business Media.
4. Banhart, J. ed., 2008. Advanced tomographic methods in materials research and engineering (Vol. 66). Oxford University Press.
5. Reyntjens, S. and Puers, R., 2001. A review of focused ion beam applications in microsystem technology. Journal of micromechanics and microengineering, 11(4), p.287.
6. Maire, E. and Withers, P.J., 2014. Quantitative X-ray tomography. International materials reviews, 59(1), pp.1-43.
7. Lehmann, E., Mannes, D., Kaestner, A. and Grünzweig, C., 2017. Recent Applications of Neutron Imaging Methods.
8. Pan, X., Sidky, E.Y. and Vannier, M., 2009. Why do commercial CT scanners still employ traditional, filtered back-projection for image reconstruction?. Inverse problems, 25(12), p.123009.
9. Stampanoni, M., Groso, A., Isenegger, A., Mikuljan, G., Chen, Q., Meister, D., Lange, M., Betemps, R., Henein, S. and Abela, R., 2007, January. TOMCAT: A beamline for TO mographic M icroscopy and C oherent r A diology experimen T s. In AIP Conference Proceedings (Vol. 879, No. 1, pp. 848-851). AIP.
10. Tkachuk, A., Duewer, F., Cui, H., Feser, M., Wang, S. and Yun, W., 2007. X-ray computed tomography in Zernike phase contrast mode at 8 keV with 50-nm resolution using Cu rotating anode X-ray source. Zeitschrift für Kristallographie-Crystalline Materials, 222(11/2007), pp.650-655.
11. Endrizzi, M., 2018. X-ray phase-contrast imaging. Nuclear Instruments and Methods in Physics Research Section A: Accelerators, Spectrometers, Detectors and Associated Equipment, 878, pp.88-98.
12. Taiwo, O.O., Finegan, D.P., Gelb, J., Holzner, C., Brett, D.J. and Shearing, P.R., 2016. The use of contrast enhancement techniques in X-ray imaging of lithium–ion battery electrodes. Chemical Engineering Science, 154, pp.27-33.
13. Pfeiffer, F., 2018. X-ray ptychography. Nature Photonics, 12(1), p.9.
14. Shearing, P.R., Gelb, J. and Brandon, N.P., 2010. X-ray nano computerised tomography of SOFC electrodes using a focused ion beam sample-preparation technique. Journal of the European Ceramic Society, 30(8), pp.1809-1814.
15. Bailey, J.J., Heenan, T.M.M., Finegan, D.P., Lu, X., Daemi, S.R., Iacoviello, F., Backeberg, N.R., Taiwo, O.O., Brett, D.J.L., Atkinson, A. and Shearing, P.R., 2017. Laser-preparation of geometrically optimised samples for X-ray nano-CT. Journal of microscopy, 267(3), pp.384-396.
16. Van Grieken, R. and Markowicz, A. eds., 2001. Handbook of X-ray Spectrometry. CRC Press.
17. Assmus, A., 1995. Early history of X rays. Beam Line, 25(2), pp.10-24.
18. B.L. Henke, E.M. Gullikson, and J.C. Davis. X-ray interactions: photoabsorption, scattering, transmission, and reflection at E=50-30000 eV, Z=1-92, Atomic Data and Nuclear Data Tables Vol. 54 (no.2), 181-342 (July 1993).
19. Hubbell, J.H. and Seltzer, S.M., 1995. Tables of X-ray mass attenuation coefficients and mass energy-absorption coefficients 1 keV to 20 MeV for elements Z= 1 to 92 and 48 additional substances of dosimetric interest (No. PB--95-220539/XAB; NISTIR--

5632). National Inst. of Standards and Technology-PL, Gaithersburg, MD (United States).
20. Alkire, C., R, Gerischer, H., Kolb, D. M., Tobias, C. W., 1990, Advances in electrochemical science and engineering, Wiley and sons.
21. Wu, J., Yuan, X.Z., Martin, J.J., Wang, H., Zhang, J., Shen, J., Wu, S. and Merida, W., 2008. A review of PEM fuel cell durability: Degradation mechanisms and mitigation strategies. Journal of Power Sources, 184(1), pp.104-119.
22. Yokokawa, H., Tu, H., Iwanschitz, B. and Mai, A., 2008. Fundamental mechanisms limiting solid oxide fuel cell durability. Journal of Power Sources, 182(2), pp.400-412.
23. Barré, A., Deguilhem, B., Grolleau, S., Gérard, M., Suard, F. and Riu, D., 2013. A review on lithium-ion battery ageing mechanisms and estimations for automotive applications. Journal of Power Sources, 241, pp.680-689.
24. Aurbach, D., Talyosef, Y., Markovsky, B., Markevich, E., Zinigrad, E., Asraf, L., Gnanaraj, J.S. and Kim, H.J., 2004. Design of electrolyte solutions for Li and Li-ion batteries: a review. Electrochimica Acta, 50(2-3), pp.247-254.
25. Mohanty, D., Li, J., Nagpure, S.C., Wood, D.L. and Daniel, C., 2015. Understanding the structure and structural degradation mechanisms in high-voltage, lithium-manganese–rich lithium-ion battery cathode oxides: A review of materials diagnostics. MRS Energy & Sustainability, 2.
26. Obrovac, M.N. and Chevrier, V.L., 2014. Alloy negative electrodes for Li-ion batteries. Chemical reviews, 114(23), pp.11444-11502.
27. Larcher, D., Beattie, S., Morcrette, M., Edstroem, K., Jumas, J.C. and Tarascon, J.M., 2007. Recent findings and prospects in the field of pure metals as negative electrodes for Li-ion batteries. Journal of Materials Chemistry, 17(36), pp.3759-3772.
28. Arora, P. and Zhang, Z., 2004. Battery separators. Chemical reviews, 104(10), pp.4419-4462.
29. Zhang, J. ed., 2008. PEM fuel cell electrocatalysts and catalyst layers: fundamentals and applications. Springer Science & Business Media.
30. Yabuuchi, N., Kubota, K., Aoki, Y. and Komaba, S., 2016. Understanding particle-size-dependent electrochemical properties of Li2MnO3-based positive electrode materials for rechargeable lithium batteries. The Journal of Physical Chemistry C, 120(2), pp.875-885.
31. Park, M., Zhang, X., Chung, M., Less, G.B. and Sastry, A.M., 2010. A review of conduction phenomena in Li-ion batteries. Journal of Power Sources, 195(24), pp.7904-7929.
32. Wang, Q., Ping, P., Zhao, X., Chu, G., Sun, J. and Chen, C., 2012. Thermal runaway caused fire and explosion of lithium ion battery. Journal of power sources, 208, pp.210-224.
33. Jung, R., Metzger, M., Maglia, F., Stinner, C. and Gasteiger, H.A., 2017. Oxygen Release and Its Effect on the Cycling Stability of LiNixMnyCozO2 (NMC) Cathode Materials for Li-Ion Batteries. Journal of The Electrochemical Society, 164(7), pp.A1361-A1377.
34. Mohanty, D., Kalnaus, S., Meisner, R.A., Rhodes, K.J., Li, J., Payzant, E.A., Wood III, D.L. and Daniel, C., 2013. Structural transformation of a lithium-rich Li1. 2Co0. 1Mn0. 55Ni0. 15O2 cathode during high voltage cycling resolved by in situ X-ray diffraction. Journal of Power Sources, 229, pp.239-248.
35. Finegan, D.P., Darcy, E., Keyser, M., Tjaden, B., Heenan, T.M., Jervis, R., Bailey, J.J., Malik, R., Vo, N.T., Magdysyuk, O.V. and Atwood, R., 2017. Characterising thermal runaway within lithium-ion cells by inducing and monitoring internal short circuits. Energy & Environmental Science, 10(6), pp.1377-1388.

36. Zhang, J. ed., 2008. PEM fuel cell electrocatalysts and catalyst layers: fundamentals and applications. Springer Science & Business Media.
37. Wang, Y., Chen, K.S., Mishler, J., Cho, S.C. and Adroher, X.C., 2011. A review of polymer electrolyte membrane fuel cells: technology, applications, and needs on fundamental research. Applied energy, 88(4), pp.981-1007.
38. Janssen, G.J.M. and Overvelde, M.L.J., 2001. Water transport in the proton-exchange-membrane fuel cell: measurements of the effective drag coefficient. Journal of Power Sources, 101(1), pp.117-125.
39. Bazylak, A., Sinton, D., Liu, Z.S. and Djilali, N., 2007. Effect of compression on liquid water transport and microstructure of PEMFC gas diffusion layers. Journal of Power Sources, 163(2), pp.784-792.
40. Holdcroft, S., 2014. Fuel Cell Catalyst Layers: A Polymer Science Perspective. Chemistry of Materials, 26, pp. 381-393.
41. Jaouen, F., Proietti, E., Lefèvre, M., Chenitz, R., Dodelet, J.P., Wu, G., Chung, H.T., Johnston, C.M. and Zelenay, P., 2011. Recent advances in non-precious metal catalysis for oxygen-reduction reaction in polymer electrolyte fuel cells. Energy & Environmental Science, 4(1), pp.114-130.
42. Trogadas, P., Cho, J.I.S., Neville, T.P., Marquis, J., Wu, B., Brett, D.J.L. and Coppens, M.O., 2018. A lung-inspired approach to scalable and robust fuel cell design. Energy & Environmental Science. 11, pp. 136-143.
43. Weber, A., 2008. Gas-Crossover and Membrane-Pinhole Effects in Polymer-Electrolyte Fuel Cells. Journal of the Electrochemical Society, 155 (6), pp. B521-B531.
44. Macauley, N., Papdias, D. D., Fairweather, J., Spernjak, D., Langlois, D., Ahluwalia, R., More, K. L., Mukundan, R. and Borup, R. L., 2018. Carbon Corrosion in PEM Fuel Cells and the Development of Accelerated Stress Tests. Journal of the Electrochemical Society, 165 (6), pp. F3148 – F3160.
45. De Bruijn, F. A., Dam, V. A. T. and Janssen, G. J. M., 2008. Review: Durability and Degradation Issues of PEM Fuel Cell Components. Fuel Cells, 1, pp. 3-22.
46. Minh, N.Q. and Takahashi, T., 1995. Science and technology of ceramic fuel cells. Elsevier.
47. Jiang, S.P., 2008. Development of lanthanum strontium manganite perovskite cathode materials of solid oxide fuel cells: a review. Journal of Materials Science, 43(21), pp.6799-6833.
48. Mori, M., Yamamoto, T., Itoh, H., Inaba, H. and Tagawa, H., 1998. Thermal Expansion of Nickel-Zirconia Anodes in Solid Oxide Fuel Cells during Fabrication and Operation. Journal of the Electrochemical Society, 145(4), pp.1374-1381.
49. Heenan, T.M.M., Robinson, J.B., Lu, X., Tjaden, B., Cervellino, A., Bailey, J.J., Brett, D.J.L. and Shearing, P.R., 2018. Understanding the thermo-mechanical behaviour of solid oxide fuel cell anodes using synchrotron X-ray diffraction. Solid State Ionics, 314, pp.156-164.
50. Robinson, J.B., Brown, L.D., Jervis, R., Taiwo, O.O., Heenan, T.M., Millichamp, J., Mason, T.J., Neville, T.P., Clague, R., Eastwood, D.S. and Reinhard, C., Lee, D., Peter, Brett, D.J.L. and Shearing, P.R., 2015. Investigating the effect of thermal gradients on stress in solid oxide fuel cell anodes using combined synchrotron radiation and thermal imaging. Journal of Power Sources, 288, pp.473-481.
51. Singhal, S.C., 2000. Advances in solid oxide fuel cell technology. Solid state ionics, 135(1-4), pp.305-313.
52. Chen, K., Chen, X., Lü, Z., Ai, N., Huang, X. and Su, W., 2008. Performance of an anode-supported SOFC with anode functional layers. Electrochimica Acta, 53(27), pp.7825-7830.

53. Zhu, W.Z. and Deevi, S.C., 2003. Development of interconnect materials for solid oxide fuel cells. Materials Science and Engineering: A, 348(1-2), pp.227-243.
54. Sarantaridis, D. and Atkinson, A., 2007. Redox Cycling of Ni-Based Solid Oxide Fuel Cell Anodes: A Review. Fuel cells, 7(3), pp.246-258.
55. Brandon, N.P. and Brett, D.J., 2006. Engineering porous materials for fuel cell applications. Philosophical Transactions of the Royal Society of London A: Mathematical, Physical and Engineering Sciences, 364(1838), pp.147-159.
56. Heenan, T.M.M., Brett, D.J.L. and Shearing, P.R., 2017, June. X-ray attenuation properties of commonly employed solid oxide fuel cell materials. In Journal of Physics: Conference Series (Vol. 849, No. 1, p. 012017). IOP Publishing.
57. Schröder, D., Bender, C.L., Arlt, T., Osenberg, M., Hilger, A., Risse, S., Ballauff, M., Manke, I. and Janek, J., 2016. Operando x-ray tomography for next-generation batteries: a systematic approach to monitor reaction product distribution and transport processes. Journal of Physics D: Applied Physics, 49(40), p.404001.
58. Zhang, H.L., Li, F., Liu, C., Tan, J. and Cheng, H.M., 2005. New insight into the solid electrolyte interphase with use of a focused ion beam. The Journal of Physical Chemistry B, 109(47), pp.22205-22211.
59. Shearing, P.R., Howard, L.E., Jørgensen, P.S., Brandon, N.P. and Harris, S.J., 2010. Characterization of the 3-dimensional microstructure of a graphite negative electrode from a Li-ion battery. Electrochemistry communications, 12(3), pp.374-377.
60. Liu, Z., Cronin, J.S., Yu-chen, K., Wilson, J.R., Yakal-Kremski, K.J., Wang, J., Faber, K.T. and Barnett, S.A., 2013. Three-dimensional morphological measurements of LiCoO2 and LiCoO2/Li (Ni1/3Mn1/3Co1/3) O2 lithium-ion battery cathodes. Journal of Power Sources, 227, pp.267-274.
61. Chen-Wiegart, Y.C.K., Liu, Z., Faber, K.T., Barnett, S.A. and Wang, J., 2013. 3D analysis of a LiCoO2–Li (Ni1/3Mn1/3Co1/3) O2 Li-ion battery positive electrode using X-ray nano-tomography. Electrochemistry Communications, 28, pp.127-130.
62. Ebner, M., Geldmacher, F., Marone, F., Stampanoni, M. and Wood, V., 2013. X-ray tomography of porous, transition metal oxide based lithium ion battery electrodes. Advanced Energy Materials, 3(7), pp.845-850.
63. Frisco, S., Kumar, A., Whitacre, J.F. and Litster, S., 2016. Understanding Li-ion battery anode degradation and pore morphological changes through nano-resolution X-ray computed tomography. Journal of The Electrochemical Society, 163(13), pp.A2636-A2640.
64. Zielke, L., Hutzenlaub, T., Wheeler, D.R., Manke, I., Arlt, T., Paust, N., Zengerle, R. and Thiele, S., 2014. A Combination of X-Ray Tomography and Carbon Binder Modeling: Reconstructing the Three Phases of LiCoO2 Li-Ion Battery Cathodes. Advanced Energy Materials, 4(8).
65. Trembacki, B.L., Mistry, A.N., Noble, D.R., Ferraro, M.E., Mukherjee, P.P. and Roberts, S.A., 2018. Editors' Choice—Mesoscale Analysis of Conductive Binder Domain Morphology in Lithium-Ion Battery Electrodes. Journal of The Electrochemical Society, 165(13), pp.E725-E736.
66. Moroni, R., Börner, M., Zielke, L., Schroeder, M., Nowak, S., Winter, M., Manke, I., Zengerle, R. and Thiele, S., 2016. Multi-scale correlative tomography of a Li-ion battery composite cathode. Scientific reports, 6, p.30109.
67. Daemi, S.R., Tan, C., Volkenandt, T., Cooper, S.J., Palacios-Padros, A., Cookson, J., Brett, D.J. and Shearing, P.R., 2018. Visualizing the Carbon Binder Phase of Battery Electrodes in Three Dimensions. ACS Applied Energy Materials, 1(8), pp.3702-3710.
68. Morelly, S.L., Gelb, J., Iacoviello, F., Shearing, P.R., Harris, S.J., Alvarez, N.J. and Tang, M.H., 2018. Three-Dimensional Visualization of Conductive Domains in Battery

Electrodes with Contrast-Enhancing Nanoparticles. ACS Applied Energy Materials, 1(9), pp.4479-4484.

69. Müller, S., Pietsch, P., Brandt, B.E., Baade, P., De Andrade, V., De Carlo, F. and Wood, V., 2018. Quantification and modeling of mechanical degradation in lithium-ion batteries based on nanoscale imaging. Nature communications, 9(1), p.2340.
70. Usseglio-Viretta, F.L., Colclasure, A., Mistry, A.N., Claver, K.P.Y., Pouraghajan, F., Finegan, D.P., Heenan, T.M., Abraham, D., Mukherjee, P.P., Wheeler, D. and Shearing, P., 2018. Resolving the Discrepancy in Tortuosity Factor Estimation for Li-Ion Battery Electrodes through Micro-Macro Modeling and Experiment. Journal of The Electrochemical Society, 165(14), pp.A3403-A3426.
71. Tan, C., Kok, M.D., Daemi, S.R., Brett, D.J. and Shearing, P.R., 2019. Three-dimensional image based modelling of transport parameters in lithium–sulfur batteries. Physical Chemistry Chemical Physics.
72. Tan, C., Heenan, T.M., Ziesche, R.F., Daemi, S.R., Hack, J., Maier, M., Marathe, S., Rau, C., Brett, D.J. and Shearing, P.R., 2018. Four-dimensional studies of morphology evolution in lithium–sulfur batteries. ACS Applied Energy Materials, 1(9), pp.5090-5100.
73. Mayo, S.C., Stevenson, A.W. and Wilkins, S.W., 2012. In-line phase-contrast X-ray imaging and tomography for materials science. Materials, 5(5), pp.937-965.
74. Babu, S.K., Mohamed, A.I., Whitacre, J.F. and Litster, S., 2015. Multiple imaging mode X-ray computed tomography for distinguishing active and inactive phases in lithium-ion battery cathodes. Journal of Power Sources, 283, pp.314-319.
75. Shearing, P.R., Brandon, N.P., Gelb, J., Bradley, R., Withers, P.J., Marquis, A.J., Cooper, S. and Harris, S.J., 2012. Multi length scale microstructural investigations of a commercially available Li-ion battery electrode. Journal of The Electrochemical Society, 159(7), pp.A1023-A1027.
76. Yufit, V., Shearing, P., Hamilton, R.W., Lee, P.D., Wu, M. and Brandon, N.P., 2011. Investigation of lithium-ion polymer battery cell failure using X-ray computed tomography. Electrochemistry Communications, 13(6), pp.608-610.
77. Robinson, J.B., Finegan, D.P., Heenan, T.M., Smith, K., Kendrick, E., Brett, D.J. and Shearing, P.R., 2018. Microstructural Analysis of the Effects of Thermal Runaway on Li-Ion and Na-Ion Battery Electrodes. Journal of Electrochemical Energy Conversion and Storage, 15(1), p.011010.
78. Chen, C., Wei, Y., Zhao, Z., Zou, Y. and Luo, D., 2019. Investigation of the swelling failure of lithium-ion battery packs at low temperatures using 2D/3D X-ray computed tomography. Electrochimica Acta.
79. Finegan, D.P., Tjaden, B., Heenan, T.M., Jervis, R., Di Michiel, M., Rack, A., Hinds, G., Brett, D.J. and Shearing, P.R., 2017. Tracking internal temperature and structural dynamics during nail penetration of lithium-ion cells. Journal of The Electrochemical Society, 164(13), pp.A3285-A3291.
80. Finegan, D.P., Darcy, E., Keyser, M., Tjaden, B., Heenan, T.M., Jervis, R., Bailey, J.J., Malik, R., Vo, N.T., Magdysyuk, O.V. and Atwood, R., 2017. Characterising thermal runaway within lithium-ion cells by inducing and monitoring internal short circuits. Energy & Environmental Science, 10(6), pp.1377-1388.2018
81. Finegan, D.P., Darcy, E., Keyser, M., Tjaden, B., Heenan, T.M., Jervis, R., Bailey, J.J., Vo, N.T., Magdysyuk, O.V., Drakopoulos, M. and Di Michiel, M., 2018. Identifying the Cause of Rupture of Li-Ion Batteries during Thermal Runaway. Advanced Science, 5(1), p.1700369.
82. Harris, S.J. and Lu, P., 2013. Effects of Inhomogeneities-Nanoscale to Mesoscale-on the Durability of Li-Ion Batteries. The Journal of Physical Chemistry C, 117(13), pp.6481-6492.

83. Cooper, S.J., Eastwood, D.S., Gelb, J., Damblanc, G., Brett, D.J.L., Bradley, R.S., Withers, P.J., Lee, P.D., Marquis, A.J., Brandon, N.P. and Shearing, P.R., 2014. Image based modelling of microstructural heterogeneity in LiFePO4 electrodes for Li-ion batteries. Journal of Power Sources, 247, pp.1033-1039.
84. Chen-Wiegart, Y.C.K., Shearing, P., Yuan, Q., Tkachuk, A. and Wang, J., 2012. 3D morphological evolution of Li-ion battery negative electrode LiVO2 during oxidation using X-ray nano-tomography. Electrochemistry Communications, 21, pp.58-61.
85. Taiwo, O.O., Paz-García, J.M., Hall, S.A., Heenan, T.M., Finegan, D.P., Mokso, R., Villanueva-Pérez, P., Patera, A., Brett, D.J. and Shearing, P.R., 2017. Microstructural degradation of silicon electrodes during lithiation observed via operando X-ray tomographic imaging. Journal of Power Sources, 342, pp.904-912.
86. Tsai, P.C., Wen, B., Wolfman, M., Choe, M.J., Pan, M.S., Su, L., Thornton, K., Cabana, J. and Chiang, Y.M., 2018. Single-particle measurements of electrochemical kinetics in NMC and NCA cathodes for Li-ion batteries. Energy & Environmental Science, 11(4), pp.860-871.
87. Villevieille, C., Ebner, M., Gómez-Cámer, J.L., Marone, F., Novák, P. and Wood, V., 2015. Influence of Conversion Material Morphology on Electrochemistry Studied with Operando X-Ray Tomography and Diffraction. Advanced Materials, 27(10), pp.1676-1681.
88. Heenan, T.M.M., Finegan, D.P., Tjaden, B., Lu, X., Iacoviello, F., Millichamp, J., Brett, D.J. and Shearing, P.R., 2018. 4D nano-tomography of electrochemical energy devices using lab-based X-ray imaging. Nano Energy, 47, pp.556-565.
89. Tan, C., Daemi, S., Taiwo, O., Heenan, T., Brett, D. and Shearing, P., 2018. Evolution of Electrochemical Cell Designs for In situ and Operando 3D Characterization. Materials, 11(11), p.2157.
90. Paz-Garcia, J.M., Taiwo, O.O., Tudisco, E., Finegan, D.P., Shearing, P.R., Brett, D.J.L. and Hall, S.A., 2016. 4D analysis of the microstructural evolution of Si-based electrodes during lithiation: Time-lapse X-ray imaging and digital volume correlation. Journal of Power Sources, 320, pp.196-203.
91. Leung, P.K., Moreno, C., Masters, I., Hazra, S., Conde, B., Mohamed, M.R., Dashwood, R.J. and Bhagat, R., 2014. Real-time displacement and strain mappings of lithium-ion batteries using three-dimensional digital image correlation. Journal of Power Sources, 271, pp.82-86.
92. Luo, J., Dai, C.Y., Wang, Z., Liu, K., Mao, W.G., Fang, D.N. and Chen, X., 2016. In situ measurements of mechanical and volume change of LiCoO2 lithium-ion batteries during repeated charge–discharge cycling by using digital image correlation. Measurement, 94, pp.759-770.
93. Finegan, D.P., Tudisco, E., Scheel, M., Robinson, J.B., Taiwo, O.O., Eastwood, D.S., Lee, P.D., Di Michiel, M., Bay, B., Hall, S.A. and Hinds, G., 2016. Quantifying Bulk Electrode Strain and Material Displacement within Lithium Batteries via High-Speed Operando Tomography and Digital Volume Correlation. Advanced Science, 3(3).
94. Eastwood, D.S., Yufit, V., Gelb, J., Gu, A., Bradley, R.S., Harris, S.J., Brett, D.J., Brandon, N.P., Lee, P.D., Withers, P.J. and Shearing, P.R., 2014. Lithiation-Induced Dilation Mapping in a Lithium-Ion Battery Electrode by 3D X-Ray Microscopy and Digital Volume Correlation. Advanced Energy Materials, 4(4).
95. Pietsch, P., Westhoff, D., Feinauer, J., Eller, J., Marone, F., Stampanoni, M., Schmidt, V. and Wood, V., 2016. Quantifying microstructural dynamics and electrochemical activity of graphite and silicon-graphite lithium ion battery anodes. Nature communications, 7, p.12909.
96. Daemi, S.R., Lu, X., Sykes, D., Behnsen, J., Tan, C., Palacios-Padros, A., Cookson, J., Petrucco, E., Withers, P.J., Brett, D.J.L. and Shearing, P.R., 2019. 4D visualisation

of in situ nano-compression of Li-ion cathode materials to mimic early stage calendering. Materials Horizons.

97. Yan, B., Lim, C., Yin, L. and Zhu, L., 2012. Three dimensional simulation of galvanostatic discharge of LiCoO2 cathode based on X-ray nano-CT images. Journal of The Electrochemical Society, 159(10), pp.A1604-A1614.
98. Kashkooli, A.G., Farhad, S., Lee, D.U., Feng, K., Litster, S., Babu, S.K., Zhu, L. and Chen, Z., 2016. Multiscale modeling of lithium-ion battery electrodes based on nano-scale X-ray computed tomography. Journal of Power Sources, 307, pp.496-509.
99. Kok, M.D., Jervis, R., Tranter, T.G., Sadeghi, M.A., Brett, D.J., Shearing, P.R. and Gostick, J.T., 2019. Mass transfer in fibrous media with varying anisotropy for flow battery electrodes: Direct numerical simulations with 3D X-ray computed tomography. Chemical Engineering Science, 196, pp.104-115.
100. Jensen, K.M., Yang, X., Laveda, J.V., Zeier, W.G., See, K.A., Di Michiel, M., Melot, B.C., Corr, S.A. and Billinge, S.J., 2015. X-ray diffraction computed tomography for structural analysis of electrode materials in batteries. Journal of The Electrochemical Society, 162(7), pp.A1310-A1314.
101. Hitchcock, A.P. and Toney, M.F., 2014. Spectromicroscopy and coherent diffraction imaging: focus on energy materials applications. Journal of synchrotron radiation, 21(5), pp.1019-1030.
102. Ulvestad, A., Singer, A., Clark, J.N., Cho, H.M., Kim, J.W., Harder, R., Maser, J., Meng, Y.S. and Shpyrko, O.G., 2015. Topological defect dynamics operando battery nanoparticles. Science, 348(6241), pp.1344-1347.
103. Yu, Y.S., Farmand, M., Kim, C., Liu, Y., Grey, C.P., Strobridge, F.C., Tyliszczak, T., Celestre, R., Denes, P., Joseph, J. and Krishnan, H., 2018. Three-dimensional localization of nanoscale battery reactions using soft X-ray tomography. Nature communications, 9(1), p.921.
104. Sinha, P.K., Halleck, P. and Wang, C.Y., 2006. Quantification of liquid water saturation in a PEM fuel cell diffusion medium using X-ray microtomography. Electrochemical and Solid-State Letters, 9(7), pp.A344-A348.
105. Krüger, P., Markötter, H., Haußmann, J., Klages, M., Arlt, T., Banhart, J., Hartnig, C., Manke, I. and Scholta, J., 2011. Synchrotron X-ray tomography for investigations of water distribution in polymer electrolyte membrane fuel cells. Journal of Power Sources, 196(12), pp.5250-5255.
106. Flückiger, R., Marone, F., Stampanoni, M., Wokaun, A. and Büchi, F.N., 2011. Investigation of liquid water in gas diffusion layers of polymer electrolyte fuel cells using X-ray tomographic microscopy. Electrochimica Acta, 56(5), pp.2254-2262.
107. Meyer, Q., Hack, J., Mansor, N., Iacoviello, F., Bailey, J. J., Shearing, P. R. and Brett, D. J. L., 2019. Multi-Scale Imaging of Polymer Electrolyte Fuel Cells using X-ray Micro- and Nano-Computed Tomography, Transmission Electron Microscopy and Helium-Ion Microscopy. Fuel Cells, 1, pp. 35-42.
108. Normile, S. J., Sabarirajan, D. C., Calzada, O., De Andrade, V., Xiao, X., Mandal, P., Parkinson, D. Y., Serov, A., Atanassov, P., Zenyuk, I. V., 2018. Direct observations of liquid water formation at nano- and micro-scale in platinum group metal-free electrodes by operando X-ray computed tomography. Materials Today Energy, 9, pp. 187-197.
109. Epting, W.K., Gelb, J. and Litster, S., 2012. Resolving the Three-Dimensional Microstructure of Polymer Electrolyte Fuel Cell Electrodes using Nanometer-Scale X-ray Computed Tomography. Advanced Functional Materials, 22(3), pp.555-560.
110. Litster, S., Epting, W.K., Wargo, E.A., Kalidindi, S.R. and Kumbur, E.C., 2013. Morphological analyses of polymer electrolyte fuel cell electrodes with nano-scale computed tomography imaging. Fuel Cells, 13(5), pp.935-945.

111. Babu, S. K., Chung, H. T., Zelenay, P. and Litster, S., 2016. Resolving Electrode Morphology's Impact on Platinum Group Metal-Free Cathode Performance Using Nano-CT of 3D Hierarchical Pore and Ionomer Distribution. ACS Applied Materials & Interfaces, 8, pp. 32764-32777.
112. James, J.P., Choi, H.W. and Pharoah, J.G., 2012. X-ray computed tomography reconstruction and analysis of polymer electrolyte membrane fuel cell porous transport layers. International Journal of Hydrogen Energy, 37(23), pp.18216-18230.
113. Gaiselmann, G., Tötzke, C., Manke, I., Lehnert, W. and Schmidt, V., 2014. 3D microstructure modeling of compressed fiber-based materials. Journal of Power Sources, 257, pp.52-64.
114. Fazeli. M., Hinebaugh, J., Fishman, Z., Tötzke, C., Lehner, W., Manke, I. and Bazylak, A., 2016. Pore network modeling to explore the effects of compression on multiphase transport in polymer electrolyte membrane fuel cell gas diffusion layers. Journal of Power Sources, 335, pp. 162-171.
115. Lee, J., Yip, R., Antonacci, P. Ge, N., Kotaka, T., Tabuchi, Y. and Bazylak, A., 2015. Synchrotron Investigation of Microporous Layer Thickness on Liquid Water Distribution in a PEM Fuel Cell. Journal of the Electrochemical Society, 162 (7), pp. F669-F676.
116. Zenyuk, I.V., Parkinson, D.Y., Hwang, G. and Weber, A.Z., 2015. Probing water distribution in compressed fuel-cell gas-diffusion layers using X-ray computed tomography. Electrochemistry Communications, 53, pp.24-28.
117. Alrwashdeh, S. S., Manke, I., Markötter, H., Klages, M., Göbel, M., Haußmann, J., Scholta, J. and Banhart, J., 2017. Operando Quantification of Three-Dimensional Water Distribution in Nanoporous Carbon-Based Layers in Polymer Electrolyte Membrane Fuel Cells. ACS Nano, 11, pp. 5944-5949.
118. Eller, J., Roth, J., Marone, F., Stampanoni, M. and Büchi, F., 2017. Operando Properties of Gas Diffusion Layers: Saturation and Liquid Permeability. Journal of the Electrochemical Society, 164 (2), pp. F115-F126.
119. Mayrhuber, I., Marone, F., Stampanoni, M., Schmidt, T. J. and Büchi, F. N., 2015. Fast X-ray Tomographic Microscopy: Investigating Mechanisms of Performance Drop during Freeze Starts of Polymer Electrolyte Fuel Cells. ChemElectroChem, 2, pp. 1551-1559.
120. Eller, J. and Büchi, F., 2013. Polymer electrolyte fuel cell performance degradation at different synchrotron beam intensities. Journal of Synchrotron Radiation, 21, pp. 82-88.
121. White, R. T., Najm, M., Dutta, M., Orfino, F. P., Kjeang, E., 2016. Communication- Effect of Micro-XCT X-ray Exposure on the Performance of Polymer Electrolyte Fuel Cells. Journal of the Electrochemical Society, 163 (10), pp. F1206-F1208.
122. Odaya, S., Phillips, R.K., Sharma, Y., Bellerive, J., Phillion, A.B. and Hoorfar, M., 2015. X-ray tomographic analysis of porosity distributions in gas diffusion layers of proton exchange membrane fuel cells. Electrochimica Acta, 152, pp.464-472.
123. Banerjee, R., Chevalier, S., Liu, H., Lee, J., Yip, R., Han, K., Hond, B. K. and Bazylak, A., 2017. A Comparison of Felt-Type and Paper-Type Gas Diffusion Layers for Polymer Electrolyte Membrane Fuel Cell Applications Using X-Ray Techniques. Journal of Electrochemical Energy Conversion and Storage, 15 (1), 011002 pp. 1-10.
124. Jinuntuya, F., Whiteley, M., Chen, R. and Fly, A., 2018. The effects of gas diffusion layers structure on water transportation using X-ray computed tomography based Lattice Boltzmann method. Journal of Power Sources, 378, pp. 53-65.
125. Meyer, Q., Mansor, N., Iacoviello, F., Cullen, P.L., Jervis, R., Finegan, D., Tan, C., Bailey, J., Shearing, P.R. and Brett, D.J.L., 2017. Investigation of Hot Pressed

Polymer Electrolyte Fuel Cell Assemblies via X-ray Computed Tomography. Electrochimica Acta, 242, pp.125-136.

126. Hinebaugh, J. and Bazylak, A., 2017. Stochastic modeling of polymer electrolyte membrane fuel cell gas diffusion layers – Part 1: Physical characterization. International Journal of Hydrogen Energy, 42(24), pp. 15861-15871.
127. Hinebaugh, J., Gostick, J. and Bazylak, A., 2017. Stochastic modeling of polymer electrolyte membrane fuel cell gas diffusion layers – Part 2: A comprehensive substrate model with pore size distribution and heterogeneity effects. International Journal of Hydrogen Energy, 42(24), pp. 15872-15886.
128. Hinebaugh, J., Fishman, Z. and Bazylak, A., 2010. Unstructured pore network modeling with heterogeneous PEMFC GDL porosity distributions. Journal of The Electrochemical Society, 157(11), pp.B1651-B1657.
129. Hasanpour, S., Hoorfar, M. and Phillion, A. B., 2017. Characterization of transport phenomena in porous transport layers using X-ray microtomography. Journal of Power Sources, 353, pp. 221-229.
130. García Salaberri, P. A., Hwang, G., Vera, M., Weber, A. Z. and Gostick, J. T., 2015. Effective diffusivity in partially saturated carbon-fiber gas diffusion layers: Effect of through-plane saturation distribution. International Journal of Heat and Mass Transfer, 86, pp. 319-333.
131. Sabharwal, M., Gostick, J. and Secanell, M., 2018. Virtual Liquid Water Intrusion in Fuel Cell Gas Diffusion Media. Journal of the Electrochemical Society, 165 (7), pp. F553-F563.
132. Zenyuk, I. V., Lamibrac, A., Eller, J., Parkinson, D. Y., Marone, F., Büchi, F. N. and Weber, A. Z., 2016. Investigating Evaporation in Gas Diffusion Layers for Fuel Cells with X-ray Computed Tomography. The Journal of Physical Chemistry C, 120, pp. 28701-28711.
133. Safi, M. A., Prasianakis, N. I., Mantzaras, J., Lamibrac, A. and Büchi, F. N., 2017. Experimental and pore-level numberical investigation of water evaporation in gas diffusion layers of polymer electrolyte fuel cells. International Journal of Heat and Mass Transfer, 115, pp. 238-249.
134. Hack, J., Heenan, T.M.M., Iacoviello, F., Mansor, N., Meyer, Q., Shearing, P., Brandon, N. and Brett, D.J.L., 2018. A Structure and Durability Comparison of Membrane Electrode Assembly Fabrication Methods: Self-Assembled Versus Hot-Pressed. Journal of The Electrochemical Society, 165(6), pp.F3045-F3052.
135. Pokhrel, A., El Hannach, M., Orfino, F.P., Dutta, M. and Kjeang, E., 2016. Failure analysis of fuel cell electrodes using three-dimensional multi-length scale X-ray computed tomography. Journal of Power Sources, 329, pp.330-338.
136. Ramani, D., Singh, Y., Orfino, F., Dutta, M. and Kjeang, E., 2018. Characterisation of Membrane Degradation Growth in Fuel Cells Using X-ray Computed Tomography. Journal of the Electrochemical Society, 165(6), pp. F3200-F3208.
137. White R. T., Wu A., Najm. M, Orfino. F.P., Dutta, M. and Kjeang, E., 2017. 4D in situ visualization of electrode morphology changes during accelerated degradation in fuel cells by X-ray computed tomography. Journal of Power Sources, 350, pp. 94-102.
138. Singh, Y., White, R. T., Najm, M., Haddow, T., Pan, V., Orfino, F. P., Dutta, M. and Kjeang, E., 2019. Tracking the evolution of mechanical degradation in fuel cell membranes using 4D in situ visualization. Journal of Power Sources, 412, pp. 224-237.
139. White, R. T., Eberhardt, S. H., Singh, Y., Haddow, T., Dutta, M., Orfino, F. P. and Kjeang, E., 2019. Four-dimensional joint visualization of electrode degradation

and liquid water distribution inside operating polymer electrolyte fuel cells. Scientific Reports, 9:1843, pp. 1-12

140. Fisher, S.L., Holmes, D., Jørgensen, J.S., Gajjar, P., Behnsen, J., Lionheart, W.R. and Withers, P.J., 2019. Laminography in the lab: imaging planar objects using a conventional x-ray CT scanner. Measurement Science and Technology.
141. Gondrom, S., Zhou, J., Maisl, M., Reiter, H., Kröning, M. and Arnold, W., 1999. X-ray computed laminography: an approach of computed tomography for applications with limited access. Nuclear engineering and design, 190(1-2), pp.141-147.
142. Saida, T., Sekizawa, O., Ishiguro, N., Hoshino, M., Uesugi, K., Uruga, T., Ohkoshi, S.I., Yokoyama, T. and Tada, M., 2012. 4D visualization of a cathode catalyst layer in a polymer electrolyte fuel cell by 3D laminography–XAFS. Angewandte Chemie International Edition, 51(41), pp.10311-10314.
143. Rehr, J.J. and Albers, R.C., 2000. Theoretical approaches to x-ray absorption fine structure. Reviews of modern physics, 72(3), p.621.
144. Ozawa, S., Matsui, H., Ishiguro, N., Tan, Y., Maejima, N., Taguchi, M., Uruga, T., Sekizawa, O., Sakata, T., Nagasawa, K. and Higashi, K., 2018. Operando Time-Resolved X-ray Absorption Fine Structure Study for Pt Oxidation Kinetics on Pt/C and Pt3Co/C Cathode Catalysts by Polymer Electrolyte Fuel Cell Voltage Operation Synchronized with Rapid O2 Exposure. The Journal of Physical Chemistry C, 122(26), pp.14511-14517.
145. Yu, L., Takagi, Y., Nakamura, T., Sakata, T., Uruga, T., Tada, M., Iwasawa, Y., Masaoka, S. and Yokoyama, T., 2018. Operando Observation of Sulfur Species Poisoning Polymer Electrolyte Fuel Cell Studied by Near Ambient Pressure Hard X-ray Photoelectron Spectroscopy. The Journal of Physical Chemistry C, 123(1), pp.603-611.
146. Uruga, T., Tada, M., Sekizawa, O., Takagi, Y., Yokoyama, T. and Iwasawa, Y., 2019. SPring-8 BL36XU: Synchrotron Radiation X-ray-based Multi-analytical Beamline for Polymer Electrolyte Fuel Cells under Operating Conditions. The Chemical Record.
147. Wilson, J.R., Kobsiriphat, W., Mendoza, R., Chen, H.Y., Hiller, J.M., Miller, D.J., Thornton, K., Voorhees, P.W., Adler, S.B. and Barnett, S.A., 2006. Three-dimensional reconstruction of a solid-oxide fuel-cell anode. Nature materials, 5(7), p.541.
148. Izzo, J.R., Joshi, A.S., Grew, K.N., Chiu, W.K., Tkachuk, A., Wang, S.H. and Yun, W., 2008. Nondestructive reconstruction and analysis of SOFC anodes using X-ray computed tomography at sub-50 nm resolution. Journal of the Electrochemical Society, 155(5), pp.B504-B508.
149. Shearing, P.R., Gelb, J. and Brandon, N., 2009. Characterization of SOFC electrode microstructure using nano-scale X-ray computed tomography and focused ion beam techniques: a comparative study. ECS Transactions, 19(17), pp.51-57.
150. Nelson, G., Harris, W., Lombardo, J., Izzo, J., Chiu, W.K., Tanasini, P., Cantoni, M., Van Herle, J., Comninellis, C., Andrews, J. and Liu, Y., 2011. Comparison of X-ray nanotomography and FIB-SEM in quantifying the composite LSM/YSZ SOFC cathode microstructure. ECS Transactions, 35(1), pp.2417-2421.
151. Nelson, G.J., Harris, W.M., Lombardo, J.J., Izzo Jr, J.R., Chiu, W.K., Tanasini, P., Cantoni, M., Comninellis, C., Andrews, J.C., Liu, Y. and Pianetta, P., 2011. Comparison of SOFC cathode microstructure quantified using X-ray nanotomography and focused ion beam–scanning electron microscopy. Electrochemistry Communications, 13(6), pp.586-589.
152. Guan, Y., Li, W., Gong, Y., Liu, G., Zhang, X., Chen, J., Gelb, J., Yun, W., Xiong, Y., Tian, Y. and Wang, H., 2011. Analysis of the three-dimensional microstructure of a solid-oxide fuel cell anode using nano X-ray tomography. Journal of Power Sources, 196(4), pp.1915-1919.

153. Laurencin, J., Quey, R., Delette, G., Suhonen, H., Cloetens, P. and Bleuet, P., 2012. Characterisation of Solid Oxide Fuel Cell Ni–8YSZ substrate by synchrotron X-ray nano-tomography: from 3D reconstruction to microstructure quantification. Journal of Power Sources, 198, pp.182-189.
154. Nelson, G.J., Grew, K.N., Izzo Jr, J.R., Lombardo, J.J., Harris, W.M., Faes, A., Hessler-Wyser, A., Wang, S., Chu, Y.S., Virkar, A.V. and Chiu, W.K., 2012. Three-dimensional microstructural changes in the Ni–YSZ solid oxide fuel cell anode during operation. Acta Materialia, 60(8), pp.3491-3500.
155. Kennouche, D., Chen-Wiegart, Y.C.K., Riscoe, C., Wang, J. and Barnett, S.A., 2016. Combined electrochemical and X-ray tomography study of the high temperature evolution of Nickel–Yttria Stabilized Zirconia solid oxide fuel cell anodes. Journal of Power Sources, 307, pp.604-612.
156. Chen-Wiegart, Y.C.K., Kennouche, D., Scott Cronin, J., Barnett, S.A. and Wang, J., 2016. Effect of Ni content on the morphological evolution of Ni-YSZ solid oxide fuel cell electrodes. Applied Physics Letters, 108(8), p.083903.
157. Shearing, P.R., Bradley, R.S., Gelb, J., Tariq, F., Withers, P.J. and Brandon, N.P., 2012. Exploring microstructural changes associated with oxidation in Ni–YSZ SOFC electrodes using high resolution X-ray computed tomography. Solid State Ionics, 216, pp.69-72.
158. Harris, W.M., Lombardo, J.J., Nelson, G.J., Lai, B., Wang, S., Vila-Comamala, J., Liu, M., Liu, M. and Chiu, W.K., 2014. Three-dimensional microstructural imaging of sulfur poisoning-induced degradation in a Ni-YSZ anode of solid oxide fuel cells. Scientific reports, 4, p.5246.
159. Heenan, T.M., Bailey, J.J., Lu, X., Robinson, J.B., Iacoviello, F., Finegan, D.P., Brett, D.J.L. and Shearing, P.R., 2017. Three-Phase Segmentation of Solid Oxide Fuel Cell Anode Materials Using Lab Based X-ray Nano-Computed Tomography. Fuel Cells, 17(1), pp.75-82.
160. Lu, X., Heenan, T.M., Bailey, J.J., Li, T., Li, K., Brett, D.J. and Shearing, P.R., 2017. Correlation between triple phase boundary and the microstructure of Solid Oxide Fuel Cell anodes: The role of composition, porosity and Ni densification. Journal of Power Sources, 365, pp.210-219.
161. Lu, X., Li, T., Taiwo, O.O., Bailey, J., Heenan, T., Li, K., Brett, D.J.L. and Shearing, P.R., 2017, June. Study of the tortuosity factors at multi-scale for a novel-structured SOFC anode. In Journal of Physics: Conference Series (Vol. 849, No. 1, p. 012020). IOP Publishing.
162. Lu, X., Tjaden, B., Bertei, A., Li, T., Li, K., Brett, D. and Shearing, P., 2017. 3D Characterization of Diffusivities and Its Impact on Mass Flux and Concentration Overpotential in SOFC Anode. Journal of The Electrochemical Society, 164(4), pp.F188-F195.
163. Heenan, T.M.M., Lu, X., Iacoviello, F., Robinson, J.B., Brett, D.J.L. and Shearing, P.R., 2018. Thermally driven SOFC degradation in 4D: Part I. Microscale. Journal of The Electrochemical Society, 165(11), pp.F921-F931.
164. Heenan, T.M.M., Lu, X., Robinson, J.B., Iacoviello, F., Brett, D.J.L. and Shearing, P.R., 2018. Thermally Driven SOFC Degradation in 4D: Part II. Macroscale. Journal of The Electrochemical Society, 165(11), pp.F932-F941.
165. Heenan, T.M., Lu, X., Finegan, D.P., Robinson, J., Iacoviello, F., Bailey, J.J., Brett, D.J.L. and Shearing, P.R., 2018. Evaluating microstructure evolution in an SOFC electrode using digital volume correlation. Sustainable Energy & Fuels, 2(12), pp.2625-2635.

166. Joshi, A.S., Grew, K.N., Peracchio, A.A. and Chiu, W.K., 2007. Lattice Boltzmann modeling of 2D gas transport in a solid oxide fuel cell anode. Journal of power sources, 164(2), pp.631-638.
167. Izzo Jr, J.R., Peracchio, A.A. and Chiu, W.K., 2008. Modeling of gas transport through a tubular solid oxide fuel cell and the porous anode layer. Journal of Power Sources, 176(1), pp.200-206.
168. Lu, X., Li, T., Bertei, A., Cho, J.I., Heenan, T.M., Rabuni, M.F., Li, K., Brett, D.J. and Shearing, P.R., 2018. The application of hierarchical structures in energy devices: new insights into the design of solid oxide fuel cells with enhanced mass transport. Energy & Environmental Science, 11(9), pp.2390-2403.
169. Grew, K.N. and Chiu, W.K., 2012. A review of modeling and simulation techniques across the length scales for the solid oxide fuel cell. Journal of Power Sources, 199, pp.1-13.
170. Yu, Y.S., Farmand, M., Kim, C., Liu, Y., Grey, C.P., Strobridge, F.C., Tyliszczak, T., Celestre, R., Denes, P., Joseph, J. and Krishnan, H., 2018. Three-dimensional localization of nanoscale battery reactions using soft X-ray tomography. Nature communications, 9(1), p.921.
171. Tsai, E.H., Billaud, J., Sanchez, D.F., Ihli, J., Odstrčil, M., Holler, M., Grolimund, D., Villevieille, C. and Guizar-Sicairos, M., 2019. Correlated X-ray 3D ptychography and diffraction microscopy visualize links between morphology and crystal structure of lithium-rich cathode materials. iScience, 11, pp.356-365.
172. Sottmann, J., Di Michiel, M., Fjellvåg, H., Malavasi, L., Margadonna, S., Vajeeston, P., Vaughan, G.B. and Wragg, D.S., 2017. Chemical Structures of Specific Sodium Ion Battery Components Determined by Operando Pair Distribution Function and X-ray Diffraction Computed Tomography. Angewandte Chemie International Edition, 56(38), pp.11385-11389.
173. Schaff, F., Bech, M., Zaslansky, P., Jud, C., Liebi, M., Guizar-Sicairos, M. and Pfeiffer, F., 2015. Six-dimensional real and reciprocal space small-angle X-ray scattering tomography. Nature, 527(7578), p.353.
174. Vamvakeros, A., Jacques, S.D.M., Di Michiel, M., Matras, D., Middelkoop, V., Ismagilov, I.Z., Matus, E.V., Kuznetsov, V.V., Drnec, J., Senecal, P. and Beale, A.M., 2018. 5D operando tomographic diffraction imaging of a catalyst bed. Nature communications, 9(1), p.4751.
175. Beale, A.M., Jacques, S.D., Gibson, E.K. and Di Michiel, M., 2014. Progress towards five dimensional diffraction imaging of functional materials under process conditions. Coordination Chemistry Reviews, 277, pp.208-223.
176. Zielke, L., Sun, F., Markötter, H., Hilger, A., Moroni, R., Zengerle, R., Thiele, S., Banhart, J. and Manke, I., 2016. Synchrotron X-ray Tomographic Study of a Silicon Electrode Before and After Discharge and the Effect of Cavities on Particle Fracturing. ChemElectroChem, 3(7), pp.1170-1177.
177. Sun, F., Markötter, H., Manke, I., Hilger, A., Kardjilov, N. and Banhart, J., 2016. Three-dimensional visualization of gas evolution and channel formation inside a lithium-ion battery. ACS applied materials & interfaces, 8(11), pp.7156-7164.
178. Vanpeene, V., Etiemble, A., Bonnin, A., Maire, E. and Roué, L., 2017. In-situ X-ray tomographic study of the morphological changes of a Si/C paper anode for Li-ion batteries. Journal of Power Sources, 350, pp.18-27.
179. Vanpeene, V., King, A., Maire, E. and Roué, L., 2019. In situ characterization of Si-based anodes by coupling synchrotron X-ray tomography and diffraction. Nano energy, 56, pp.799-812.
180. Wu, J., Zhu, X., West, M. M., Tyliszczak, T., Shiu, H-W., Shapiro, D., Berejnov, V., Susac, D., Stumper, J. and Hitchcock, A. P., 2018. High-resolution imaging of

polymer electrolyte membrane fuel cell cathode layers by soft X ray spectro ptychography. Journal of Physical Chemistry C, 122, pp. 11709-11719.

181. Matsui, H., Ishiguro, N., Uruga, T., Sekizawa, O., Higashi, K., Maejima, N. and Tada, M., 2017. Operando 3D visualisation of migration and degradation of a platinum cathode catalyst in a polymer electrolyte fuel cell. Angewandte Chemie International Edition, 56, pp. 9371-9375.

182. Garbayo, I., Baiutti, F., Morata, A. and Tarancón, A., 2019. Engineering mass transport properties in oxide ionic and mixed ionic-electronic thin film ceramic conductors for energy applications. Journal of the European Ceramic Society, 39(2-3), pp.101-114.

183. Li, T., Heenan, T.M., Rabuni, M.F., Wang, B., Farandos, N.M., Kelsall, G.H., Matras, D., Tan, C., Lu, X., Jacques, S.D. and Brett, D.J., 2019. Design of next-generation ceramic fuel cells and real-time characterization with synchrotron X-ray diffraction computed tomography. Nature communications, 10(1), p.1497.

184. Walker, R.C., Shi, T., Silva, E.C., Jovanovic, I. and Robinson, J.A., 2016. Radiation effects on two-dimensional materials. physica status solidi (a), 213(12), pp.3065-3077.

185. Abellan, P., Mehdi, B.L., Parent, L.R., Gu, M., Park, C., Xu, W., Zhang, Y., Arslan, I., Zhang, J.G., Wang, C.M. and Evans, J.E., 2014. Probing the degradation mechanisms in electrolyte solutions for Li-ion batteries by in situ transmission electron microscopy. Nano letters, 14(3), pp.1293-1299.

186. Maire, E. and Withers, P.J., 2014. Quantitative X-ray tomography. International materials reviews, 59(1), pp.1-43.

187. Rahwan, I., Cebrian, M., Obradovich, N., Bongard, J., Bonnefon, J.F., Breazeal, C., Crandall, J.W., Christakis, N.A., Couzin, I.D., Jackson, M.O. and Jennings, N.R., 2019. Machine behaviour. Nature, 568(7753), p.477.

188. Berecibar, M., 2019. Machine-learning techniques used to accurately predict battery life. Nature 568, pp. 325-326